



3.1 Modified Cam Clay Model with Drained Condition

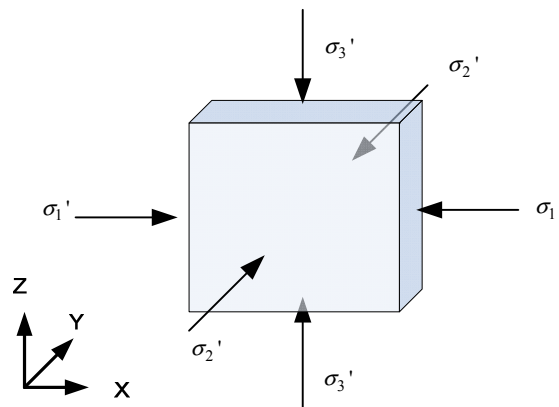
REFERENCE	Sam Helwany ¹
ELEMENTS	Solid elements
MODEL FILENAME	Material01.gts

Nonlinear tri-axial tension and compression are carried out using modified Cam-clay model with drained condition. The objective of this example is to verify the material model in reproducing the theoretical effective pressure-shear stress response. The theoretical response can be obtained analytically from the following set of equations:

$$\begin{aligned} \sigma_1' &= \sigma_2' \neq \sigma_3' \\ p' &= -\frac{\sigma_1' + \sigma_2' + \sigma_3'}{3} \\ q &= |\sigma_3' - \sigma_1'| \\ \frac{\Delta q}{\Delta p'} &= 3 \end{aligned}$$

Tri-axial tension and compression tests are performed for normally consolidated and over-consolidated soil specimen as depicted in Figure 3.1.1. Initial stage is set up where pressure is applied along the x-, y- and z-directions to reproduce the in-situ stresses. In the subsequent stage, additional pressure is applied in the z-direction for loading test. For the unloading case, specified displacement load is applied in the z-direction.

Figure 3.1.1
Drained tri-axial test





Material data	Poisson's ratio	$\nu = 0.3$
	<i>OCR</i>	1.0 : normal consolidation 2.0 : over consolidation
	κ	0.026
	λ	0.174
	e_0	0.889
	M	1.0
	<i>Drained</i>	

Figure 3.1.2
Mean effective pressure vs. shear stress for loading/unloading in normal consolidation condition

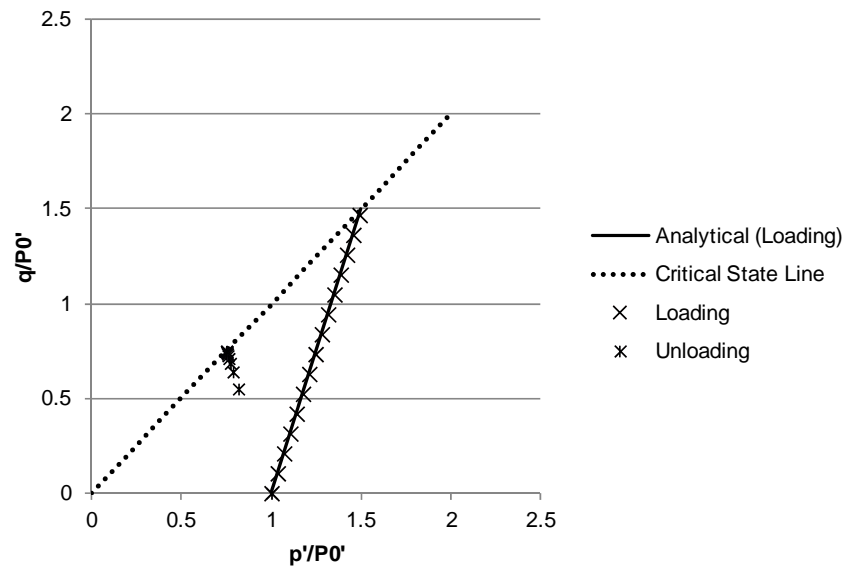


Figure 3.1.3
Axial strain vs. shear stress for loading/unloading in normal consolidation condition

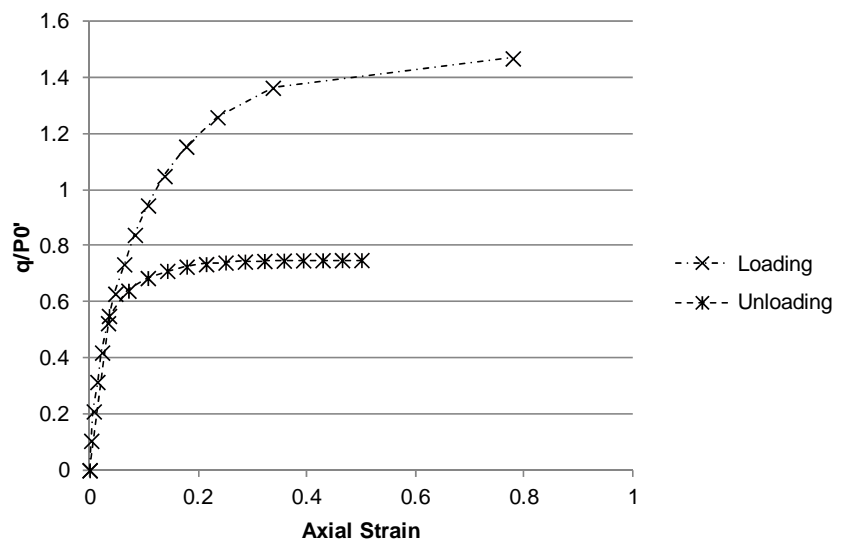




Figure 3.1.4
Mean effective pressure vs. shear stress for loading/unloading in over-consolidation condition (OCR=2)

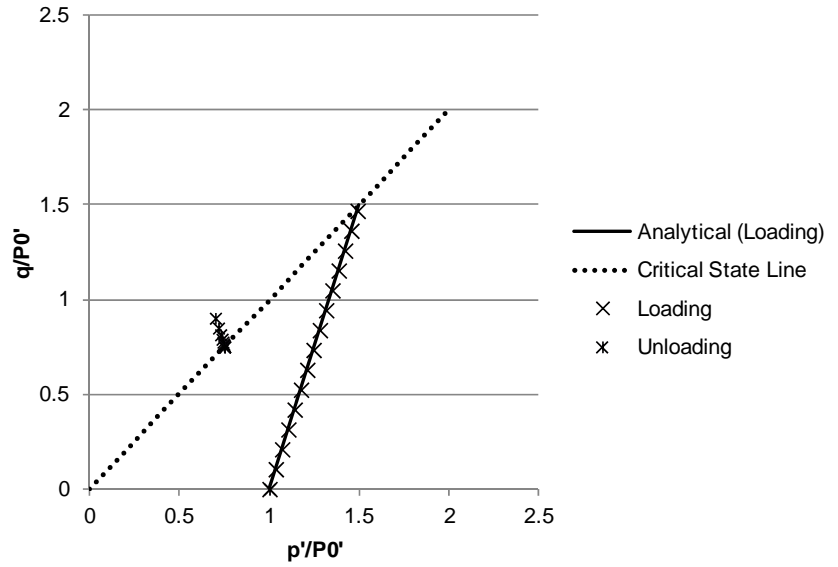
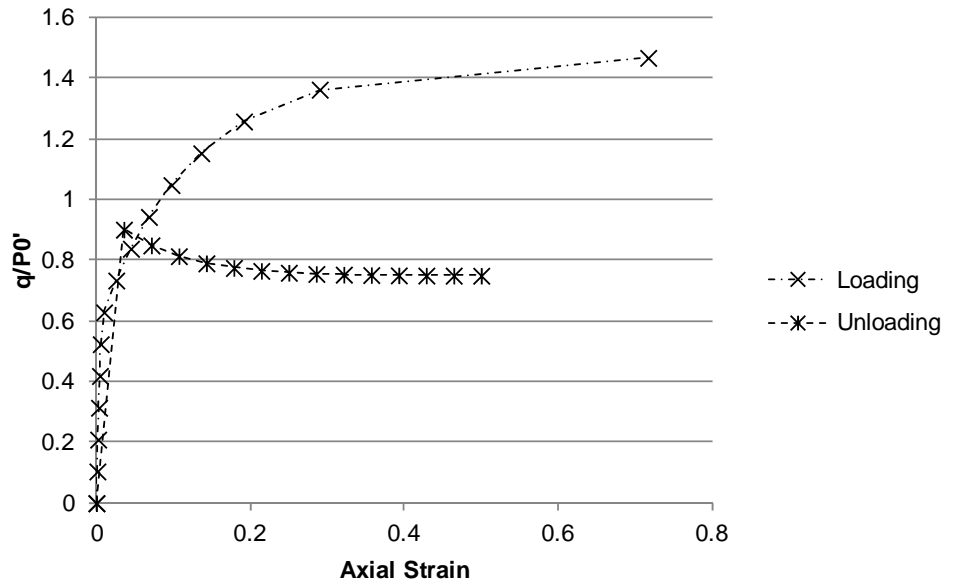


Figure 3.1.5
Axial strain vs. shear stress for loading/unloading in over-consolidation condition (OCR=2)





3.2 Modified Cam Clay Model with Undrained Condition

REFERENCE	Wood, D. M. ²
ELEMENTS	Solid elements
MODEL FILENAME	Material02-A.gts, Material02-B.gts

Nonlinear tri-axial compression tests are carried out using modified Cam-clay model with undrained condition. The objective of this example is to verify the material model in reproducing the theoretical effective pressure-shear stress response in undrained condition. The theoretical response can be obtained analytically from the following set of equations:

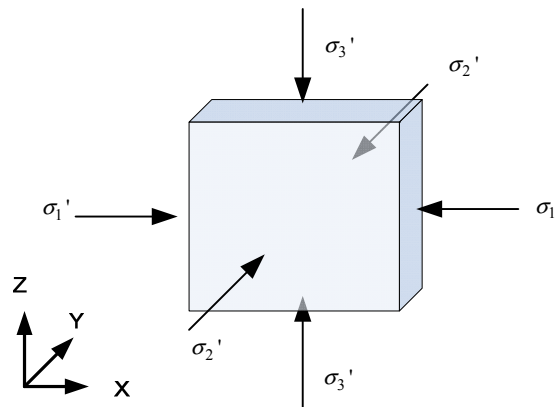
$$\frac{p_i'}{p'} = \left(\frac{M^2 + \eta^2}{M^2 + \eta_i^2} \right)^\Lambda$$

$$\Lambda = \frac{\lambda - \kappa}{\lambda}$$

$$\eta = \frac{q}{p'}$$

p_i' , η_i define the effective stress state at impending yield. Tri-axial compression tests are performed for over-consolidated soil specimen as depicted in Figure 3.2.1. Initial stage is set up where pressure is applied along the x-, y- and z-directions to reproduce the in-situ stresses. In the subsequent stage, additional displacement load is applied in the z-direction for loading test.

Figure 3.2.1
Undrained tri-axial test





Material data	Poisson's ratio	$\nu = 0.3$
	<i>OCR</i>	1.5
		2.5
	κ	0.026
	λ	0.174
	e_0	0.889
	M	1.0
<i>Undrained</i>		

Figure 3.2.2
Mean pressure vs. shear stress for loading in over consolidation condition (OCR=1.5)

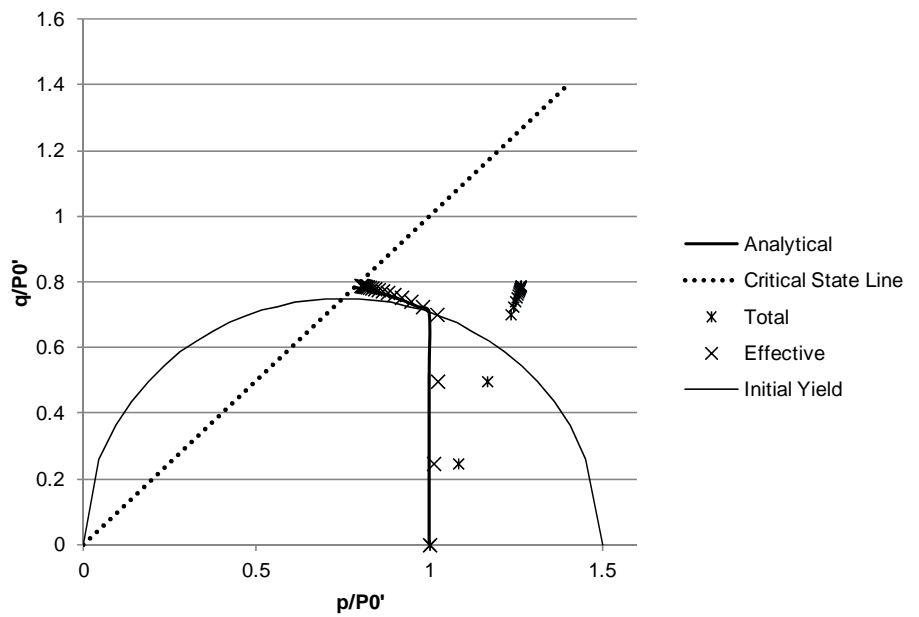
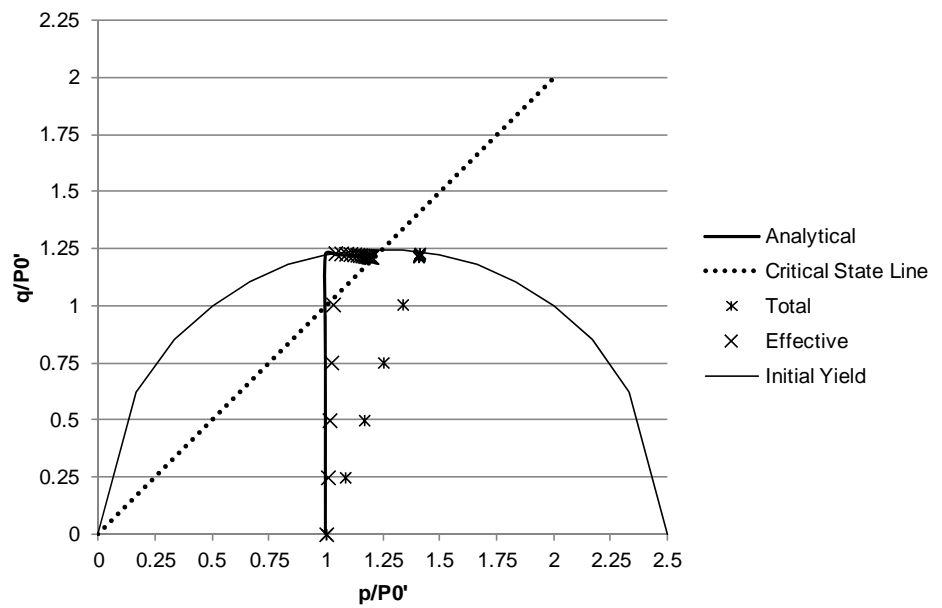


Figure 3.2.3
Mean pressure vs. shear stress for loading in over consolidation condition (OCR=2.5)





3.3 Internally Pressurized Spherical Shell Composed of von-Mises Material

REFERENCE	Hill, R. ³
ELEMENTS	Solid elements, axisymmetric elements
MODEL FILENAME	Material03_1.gts, Material03_2.gts

A spherical shell model is depicted in Figure 3.3.1. The model is composed of the elastic-perfectly plastic von Mises material model. The model is subjected to a uniform internally pressure P . Nonlinear analysis is carried out with arc-length method to obtain the pressure-deflection response. Solutions are obtained using both solid and axisymmetric elements. The inner and outer radii (a and b) are 1m and 2m, respectively.

Analytical solution derived by Hill is adopted for comparison. The closed form solution for the pressure-deflection relations can be represented as:

$$\begin{cases} u_b = \frac{3Pb}{2E(b^3/a^3 - 1)}(1-\nu) & (P < P_0) \\ u_b = \frac{\sigma_{y_0} c^3}{Eb^2}(1-\nu) & (P \geq P_0) \end{cases}$$

where P_0 is the pressure at the onset of plasticity and plastic radius, c can be obtained from:

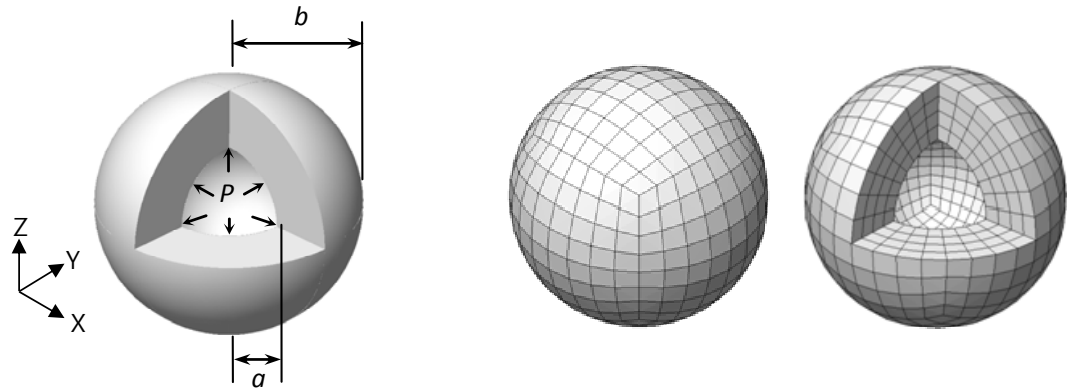
$$P = 2\sigma_{y_0} \ln\left(\frac{c}{a}\right) + \frac{2\sigma_{y_0}}{3} \left(1 - \frac{c^3}{b^3}\right)$$

The limiting load is reached when $c = b$, and can be represented as:

$$P_{\text{lim}} = 2\sigma_{y_0} \ln\left(\frac{b}{a}\right)$$

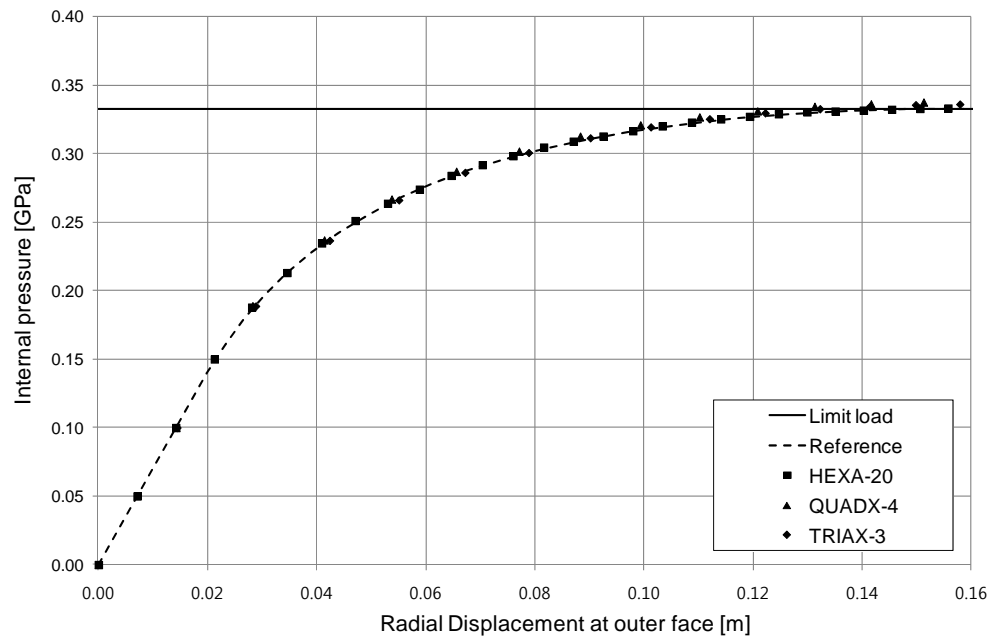


Figure 3.3.1
Geometry and mesh of spherical shell model



Material data	Young's modulus	$E = 21.0 \text{ GPa}$
	Poisson's ratio	$\nu = 0.3$
	Yield criteria	<i>von-Mises</i>
	Yield stress	240 MPa

Figure 3.3.2
Graph of internal pressure vs. radial displacement at outer face



*Table 3.3.1 Limit pressure obtained using solid and axisymmetric elements*

	P_{inter} [GPa]
Reference	0.3327
HEXA-20	0.3200
QUADX-4	0.3396
QUADX-8	0.3396
TRIAX-3	0.3368
TRIAX-6	0.3328



3.4 A V-notch Bar composed of Elastic-Perfectly Plastic Tresca Material Model

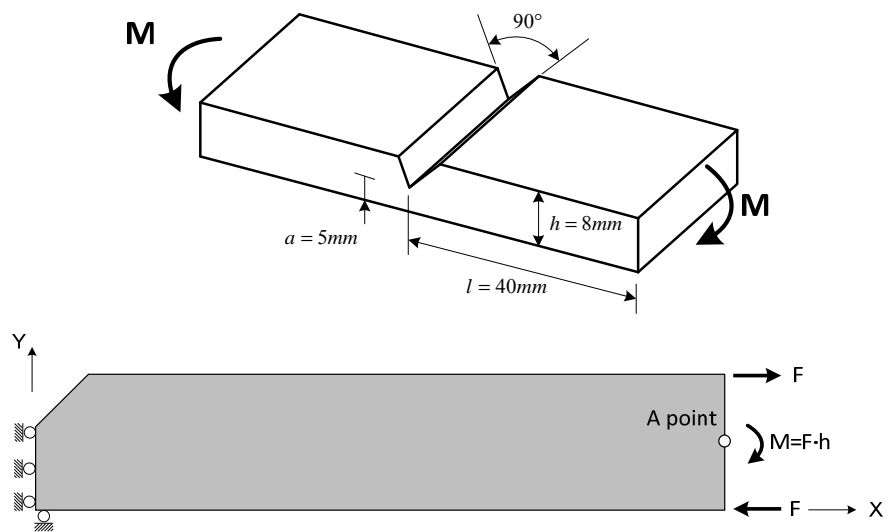
REFERENCE	Green, A.P. ⁴ , Chakrabarty, J. ⁵
ELEMENTS	Plane strain elements
MODEL FILENAME	Material04.gts

A wide rectangular metal bar containing a deep 90° V-shaped notch subjected to pure bending is considered. Figure 3.4.1, shows the geometry of the model. The model is considered as a plain strain problem. Elastic-perfectly plastic Tresca material behavior is assumed. The bending moment is applied by means of two opposite nodal forces as indicated in Figure 3.4.1. 8-node quadrilateral plane strain elements are used for the nonlinear analysis. Utilizing the symmetry of the problem, only half of the model is analyzed with symmetric boundary conditions enforced. The obtained bending moment is compared with an analytic solution. The analytic solution for the upper bound of the moment per unit width is available based on the theory of slip line field:

$$M_u \approx 0.623ca^2$$

where a is the thickness of the bar in the neck and c is the shear strength, which for the Tresca material model is half of the yield stress, $c = \sigma_Y / 2$

Figure 3.4.1 V-shaped notch problem



Material data	Young's modulus	$E = 210000 \text{ MPa}$
	Poisson's ratio	$\nu = 0.3$
	Yield criteria	<i>Tresca</i>
	Yield Stress	240 MPa



Figure 3.4.2
Normalized bending moment obtained using plane strain elements

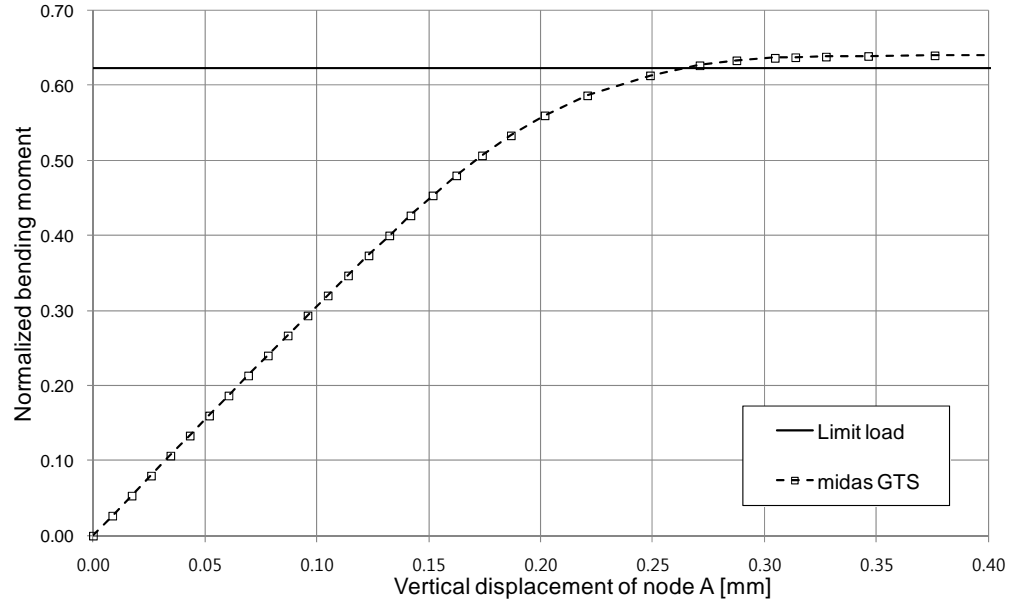


Table 3.4.1 Normalized bending moment

	Normalized bending moment
Reference	0.623
QUAD-8	0.641

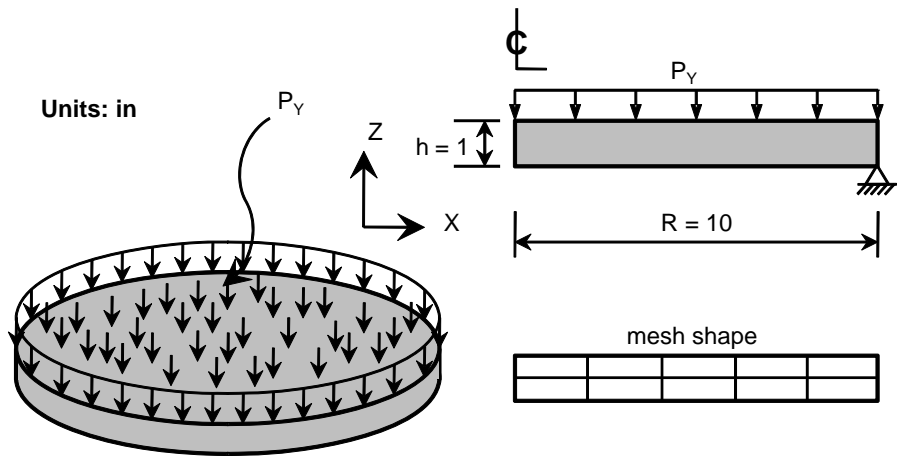


3.5 Uniformly Loaded Circular Plate

REFERENCE	Owen et al. ⁶
ELEMENTS	Axisymmetric elements
MODEL FILENAME	Material05.gts

Figure 3.5.1 shows a circular plate model simply supported around its outer rim under uniform pressure. The circular plate exhibits material nonlinear behavior. The constitutive model follows the elastic-perfectly plastic von Mises model. The limit pressure is determined using various types of axisymmetric elements.

Figure 3.5.1
Circular plate model



Material data	Young's modulus	$E = 1.0 \times 10^7 \text{ psi}$
	Poisson's ratio	$\nu = 0.24$
	Model type	<i>Von-Mises</i>
	Yield stress	16000.0 psi
Load data	Nodal Force	264 lbf/in



Figure 3.5.2
Pressure vs. center
deflection of circular
plate model obtained
using axisymmetric
elements

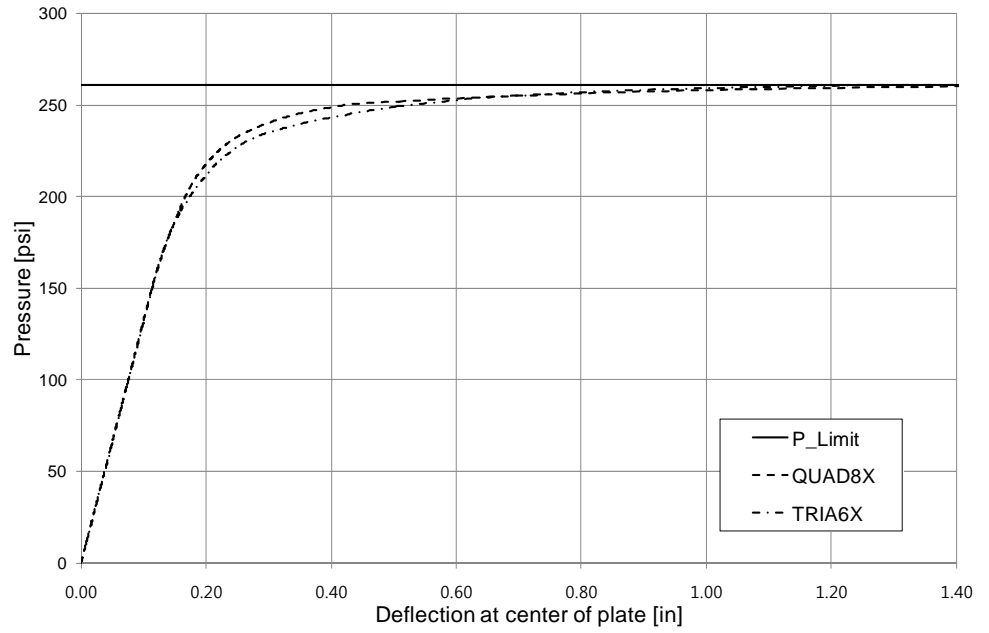


Table 3.5.1 Limit pressure

	$P_{lim} [psi]$
Reference	260.8
QUAD-8	261.2
TRIA-6	261.4

$$* P_{lim} \approx \frac{6.52M_y}{R^2}, \quad M_y \equiv \frac{\sigma_y h^2}{4}$$

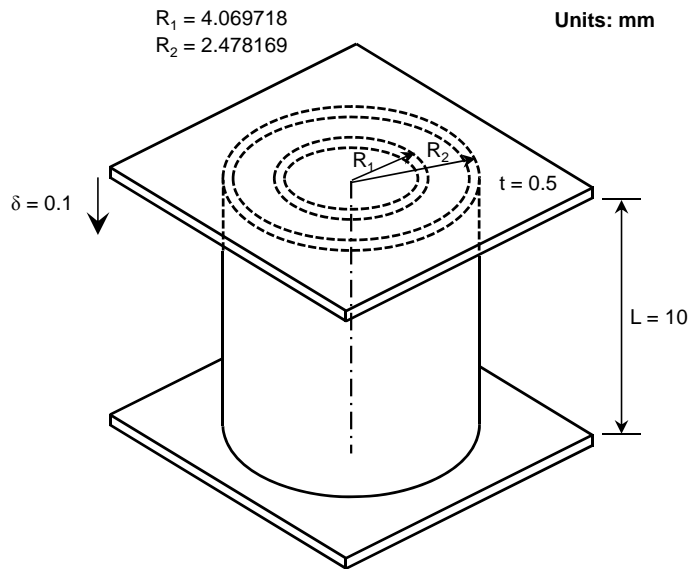


3.6 Two Coaxial Tubes

REFERENCE	Crandall et al. ⁷
ELEMENTS	Solid elements
MODEL FILENAME	Material06.gts

Figure 3.6.1 shows two coaxial tubes made out of steel (1020-CR) and aluminum alloy (2024-T4) compressed between two rigid flat ends. Both tubes are assumed to follow the von Mises elastic-perfectly plastic material model with the associated flow rule.

Figure 3.6.1
Two coaxial tubes



Material data (Inner tube: steel 1020-RC)	Young's modulus	$E_{steel} = 1.84375 \times 10^5 \text{ N/mm}^2$
	Poisson's ratio	$\nu_{steel} = 0.3$
	Model type	von-Mises
	Yield stress	590 N/mm^2
Material data (Outer tube: aluminum alloy 2024-T4)	Young's modulus	$E_{alloy} = 7.6 \times 10^4 \text{ N/m}^2$
	Poisson's ratio	$\nu_{alloy} = 0.3$
	Model type	von-Mises
	Yield stress	380 N/mm^2
Load data	Prescribed displacement	0.1 mm



Figure 3.6.2
Reaction force vs.
applied displacement
curve obtained using
hexahedron elements

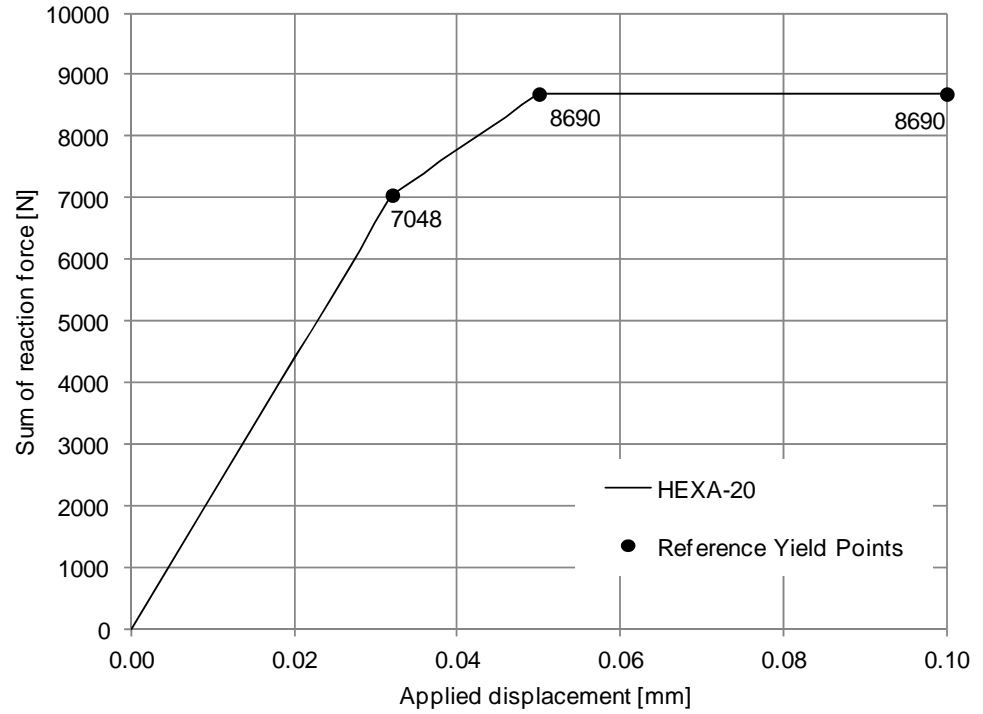


Table 3.6.1 Reaction force at the bottom surface with the entire model at plasticity state

	F_R [N]
Reference	8690.0
HEXA-8	8681.1
PENTA-6	8673.3
HEXA-20	8681.1
PENTA-15	8683.7

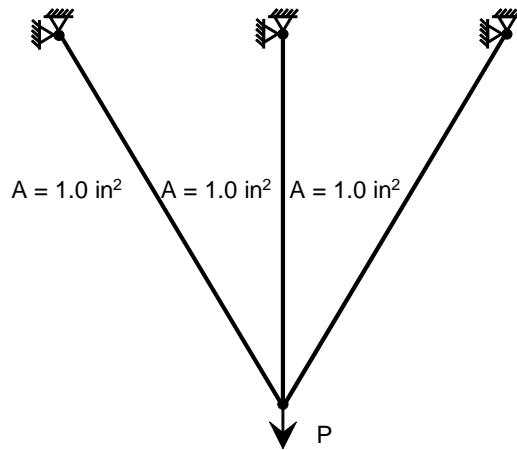


3.7 Residual Stress Problem

REFERENCE	Crandall et al. ⁷
ELEMENTS	Truss elements
MODEL FILENAME	Material07.gts

Figure 3.7.1 shows a chain hoist attached to the ceiling through three tie trusses, which are made out of cold-rolled steel with the yield strength of σ_y . The three-truss structure is loaded in the vertical direction and then unloaded. While the structure is loaded, the center truss member yields first while the side members remain elastic. When the frame is fully loaded, all the three trusses become fully plastic.

Figure 3.7.1
Three member truss model



Material data	Young's modulus	$E = 30.0 \times 10^6 \text{ psi}$
	Poisson's ratio	$\nu = 0.3$
	Model type	<i>von-Mises</i>
	Yield stress	30000.0 psi
Section Property	Cross-sectional area	$A = 1.0 \text{ in}^2$



Figure 3.7.2
Stress-deflection curve
of the center member

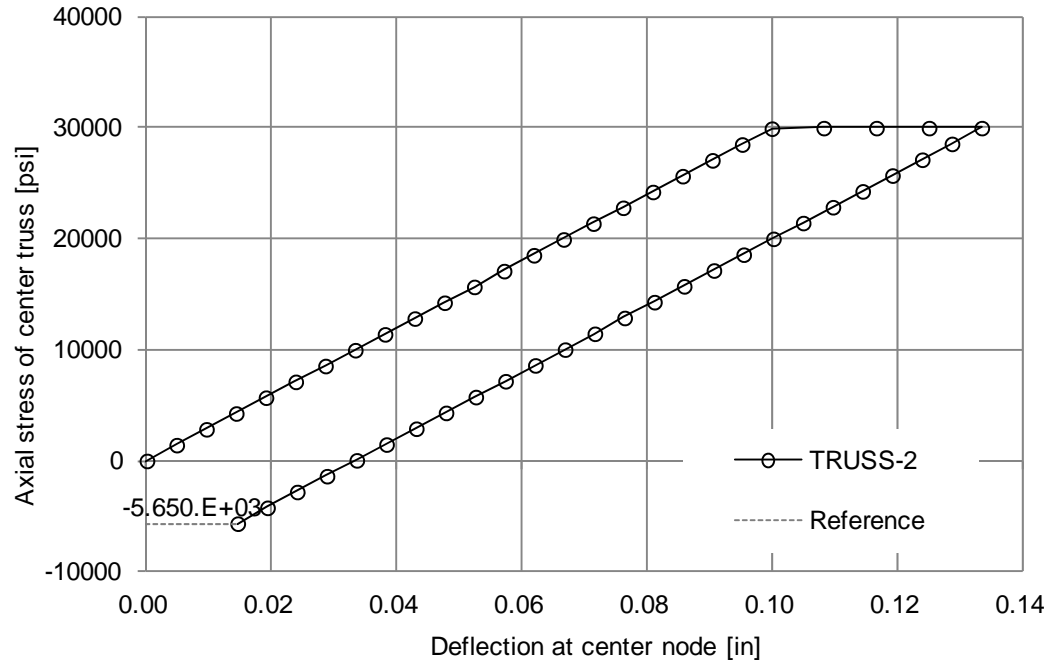


Table 3.7.1 Residual stress results of center member after loading-unloading

	$\delta_{elastic}$ [in]	σ_{res} [psi]
Reference	0.1000	-5650
TRUSS-2	0.0998	-5650



3.8 End-Loaded Tapered Cantilever Composed of Tresca Material Model

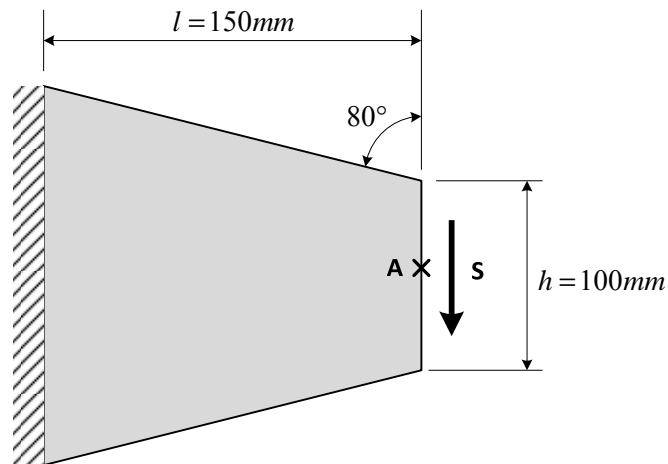
REFERENCE	Green, A.P. ⁸
ELEMENTS	Plane strain elements, Tresca
MODEL FILENAME	Material08.gts

Figure 3.8.1 shows a cantilevered tapered beam subjected to uniform shear force at the free edge. Elastic-perfectly plastic Tresca material model behavior is assumed. The cantilever problem is discretized using plane strain elements to obtain the limit load. Comparison is made with an analytical solution based on the theory of slip line field. The normalized upper bound for shear pressure is expressed as:

$$\frac{S_u}{c} \approx 0.775$$

where c is the shear strength, which for the Tresca material model is half of the yield stress, $c = \sigma_Y / 2$

Figure 3.8.1
End-loaded tapered
cantilever model



Material data	Young's modulus	$E = 210000 \text{ MPa}$
	Poisson's ratio	$\nu = 0.3$
	Yield criteria	<i>Tresca</i>
	Yield stress	240 MPa
Section data	Plane strain	



Figure 3.8.2
Normalized load vs.
normalized edge
deflection of tapered
beam model using
plane strain elements

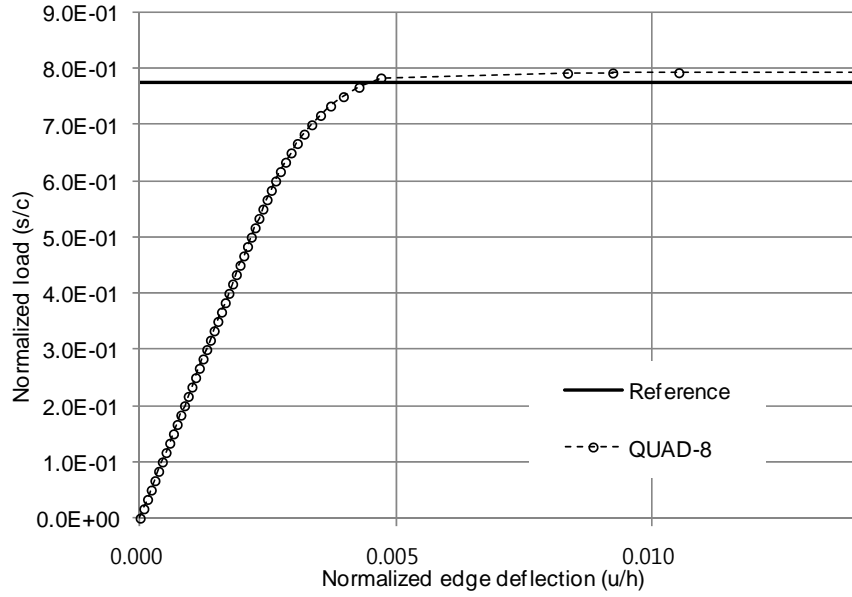


Table 3.8.1 Normalized bending moment compared with analytical solution

	Normalized bending moment
Reference	0.775
QUAD-8	0.798

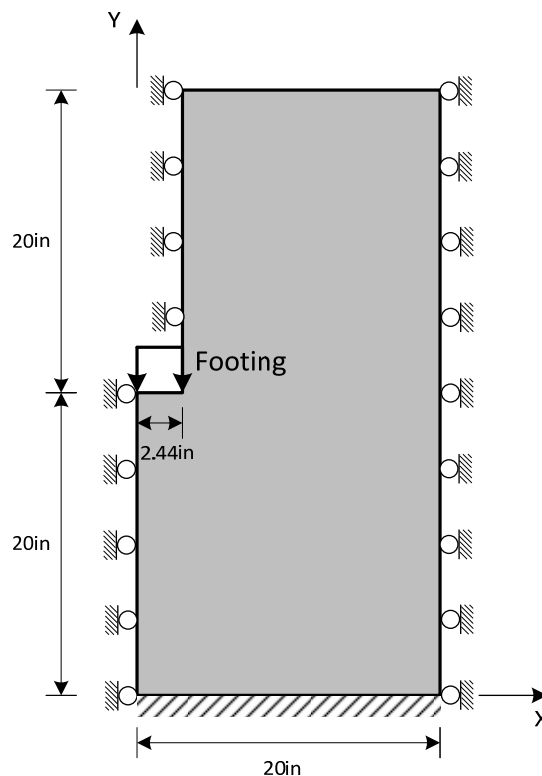


3.9 Strip Footing in Sand

REFERENCE	Duncan, J. M. et al. ⁹
ELEMENTS	Plane strain elements, Footing, Cohesion varying
MODEL FILENAME	Material09.gts

Figure 3.9.1 shows the symmetric computational model for the strip footing in sand. Duncan-Chang material behavior is assumed. Nonlinear finite element analysis is carried out where prescribed displacement is applied on the footing surface. Plane strain elements are used to obtain the pressure vs. settlement response. The results are compared with computational solution and experimental observations found in the reference.

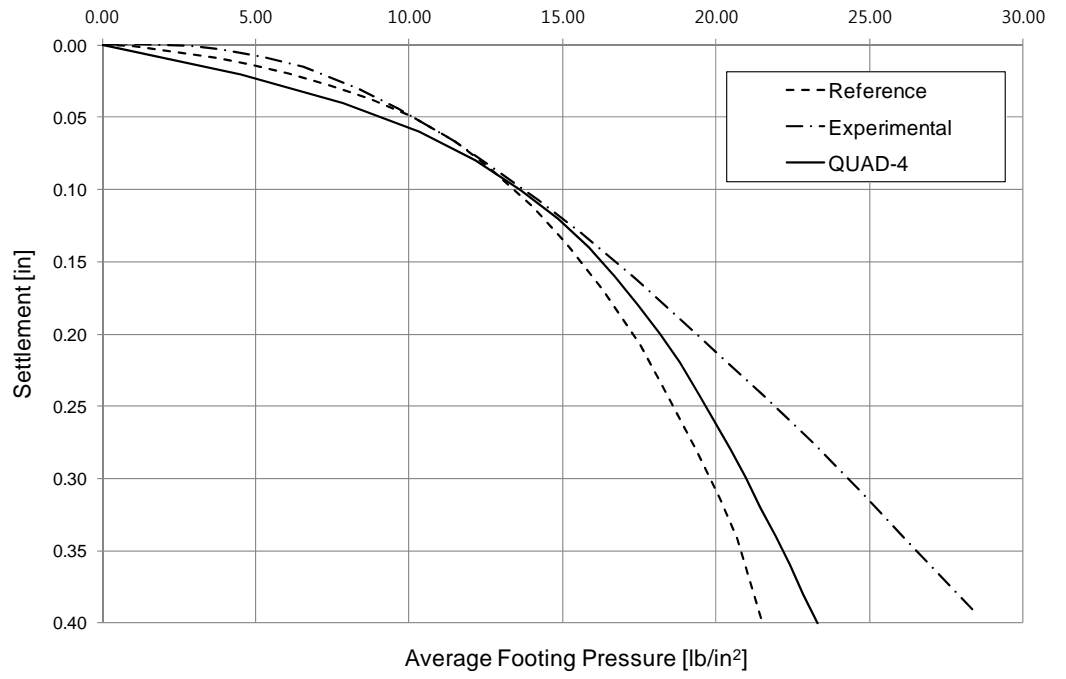
Figure 3.9.1
Half model of strip footing
problem



Material data	Model Type	<i>Hyperbolic (Duncan-Chang)</i>
	Initial loading modulus	$K = 300$
	Initial stiffness ratio	$n = 0.55$
	Failure Ratio	$R_f = 0.83$
	Cohesion	$C = 0$
	Friction angle	$\phi = 35.5^\circ$
	Unit Weight	$91 \text{ lb} / \text{ft}^3$
	Poisson ratio	$\nu = 0.35$



Figure 3.9.2
Settlement vs. average
footing pressure obtained
using plane strain
elements





3.10 Bearing Capacity of Smooth Square Footing on a Frictionless Material

REFERENCE	Shield et al. ¹⁰ , Chen ¹¹
ELEMENTS	Solid elements
MODEL FILENAME	Material10.gts

Figure 3.10.1 shows a quarter model of a square footing problem on a frictionless material. Nonlinear finite element analysis is carried out to determine the bearing capacity of the problem with symmetric boundary conditions imposed on the planes of symmetry. Smooth footing is simulated by prescribing displacements in the vertical direction while releasing the displacements in the horizontal directions. Mohr-Coulomb material model with zero friction and dilatancy angles is used to model the material behavior.

For comparison, the upper and lower bounds for the bearing capacity are taken, which are available in the reference in the following form:

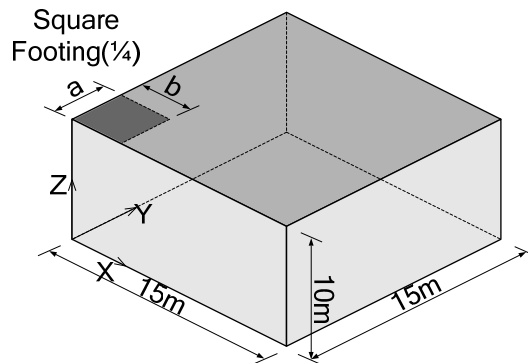
$$q_{\max} = c \left(5.24 + 0.47 \frac{a}{b} \right) \quad \frac{a}{b} \geq 0.53$$

$$q_{\max} = c \left(5.14 + 0.66 \frac{a}{b} \right) \quad \frac{a}{b} < 0.53$$

$$q_{\min} = c(2 + \pi)$$

where c is the cohesion of the material.

Figure 3.10.1
Quarter symmetry
model of square footing
problem





Material data	Young's modulus	$E = 257142.9 \text{ kPa}$
	Poisson's ratio	$\nu = 0.285714$
	Yield criteria	<i>Mohr-Coulomb</i>
	Cohesion	$c = 100 \text{ kPa}$
	Friction angle	$\phi = 0^\circ$
	Dilatancy angle	$\psi = 0^\circ$

Figure 3.10.2
Bearing pressure vs. applied displacement for square footing problem obtained using solid elements

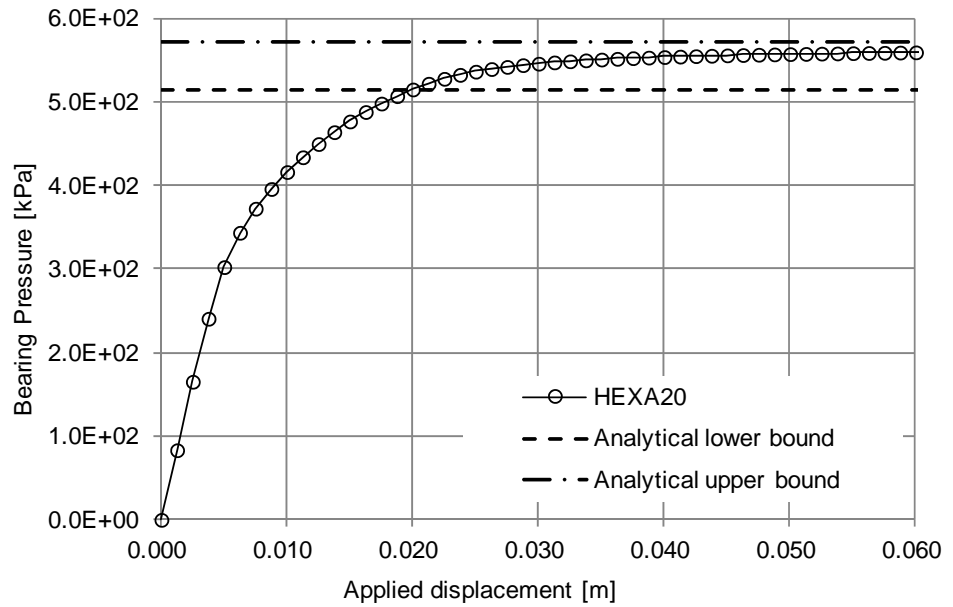


Table 3.10.1 Bearing capacity of square footing problem (F_z)

Collapse Load	F_z [kPA] at upper bound	F_z [kPA] at lower bound
Reference	571.0	514.2
HEXA-20		560.3



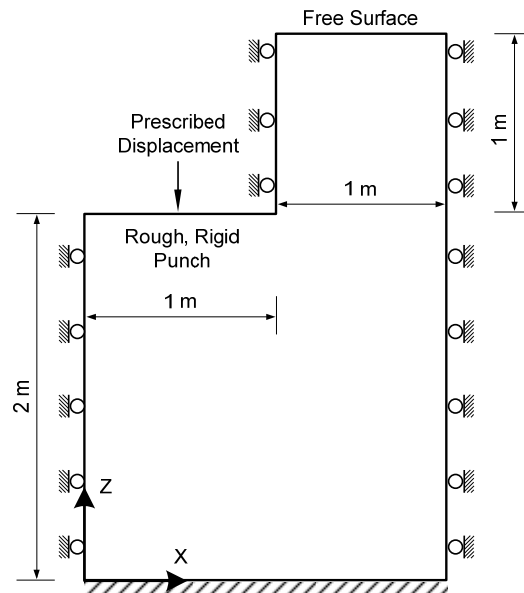
3.11 Rigid Punch Penetrating into Clay

REFERENCE	Van Langen, H. et al. ¹²
ELEMENTS	Plane strain elements, Footing, Cohesion varying
MODEL FILENAME	Material11.gts

Figure 3.11.1 depicts a rigid punch penetrating into clay. The base of the punch is assumed to be fully rough whereas the side is fully smooth. The constitutive behavior of the material is elastic-perfectly plastic Tresca model. Nonlinear static analysis is carried out with the punch penetration modeled as vertical displacements prescribed at the base of the punch. The rough base is taken into account by constraining horizontal displacements at the base of the punch.

The resulting limit pressure is compared with an analytical solution based on slip line field theory. The limiting pressure for the dimension shown in Figure 3.11.1 is expressed as, $p = (\pi + 2)c$ where c is the cohesion of the material.

Figure 3.11.1
Geometry and boundary conditions of the rigid punch penetration problem



Material data	Young's modulus	$E = 2500 \text{ kPa}$
	Poisson's ratio	$\nu = 0.25$
	Yield criteria	<i>Mohr-Coulomb</i>
	Cohesion	$c = 10 \text{ kPa}$
	Friction angle	$\phi = 0^\circ$
	Dilatancy angle	$\psi = 0^\circ$



Figure 3.11.2
Average pressure vs.
applied displacement
obtained using plane
strain elements

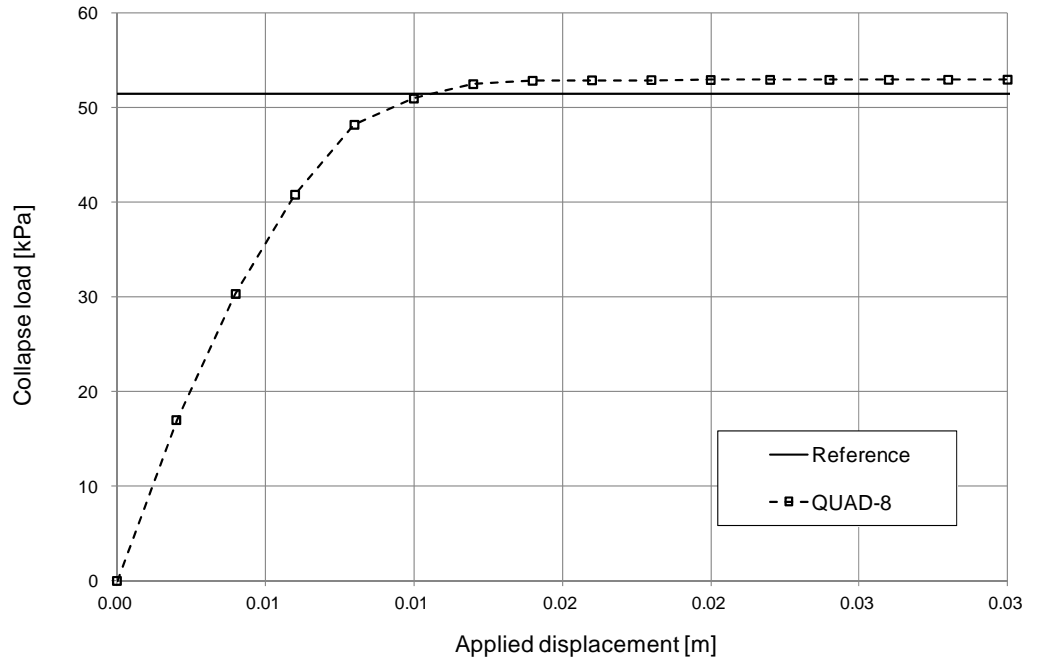


Table 3.11.1 Collapse load for 8-element punch

Collapse load	F_z [kN] at punch
Reference	51.42
QUAD-8	52.97



3.12 Cylindrical Hole in an Infinite Mohr-Coulomb Medium

REFERENCE	Salencon, J ¹³
ELEMENTS	Plane strain elements, axisymmetric elements
MODEL FILENAME	Material12_1.gts, Material12_2.gts

Cylindrical hole in an infinite medium is considered. The infinite medium is subjected to in-situ normal stress of -30MPa aligned with the axes as shown in Figure 3.12.1. The constitutive behavior of the material is elastic-perfectly plastic Mohr-Coulomb model. Nonlinear static analysis is carried out with both plane strain and axisymmetric elements. The plane strain approach models the infinite medium as a square with side length of 20m and discretizes quarter of the model utilizing symmetry. The axisymmetric approach models the medium as a cylinder with radius of 10 m. The distribution of stresses and displacements along the radius are compared with an analytical solution.

Figure 3.12.1
Quarter model of
cylindrical hole

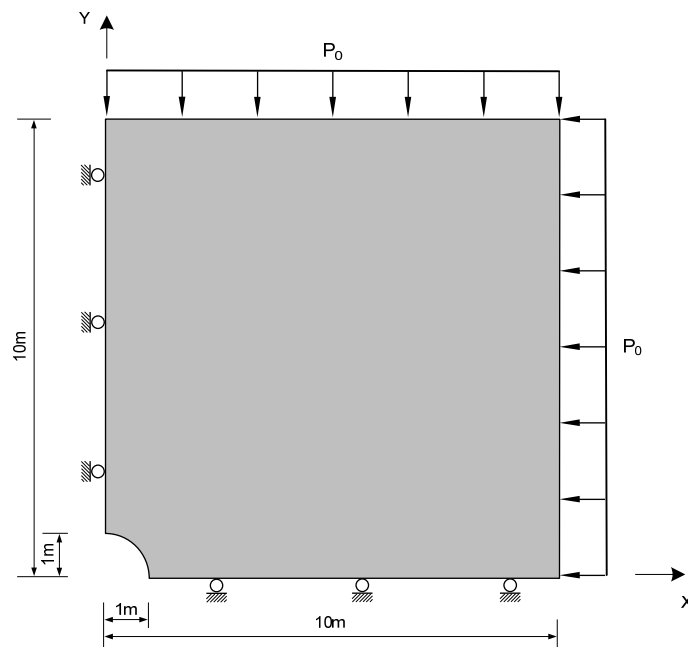
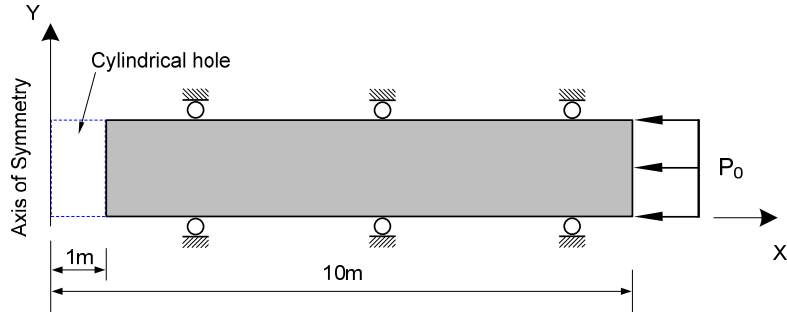




Figure 3.12.2
Axisymmetric model of cylindrical hole



Material data	Young's modulus	$E = 6777.931 \text{ MPa}$
	Poisson's ratio	$\nu = 0.210345$
	Yield criteria	<i>Mohr-Coulomb</i>
	Cohesion	$c = 3.45 \text{ MPa}$
	Friction angle	$\phi = 30^\circ$
	Dilatancy angle	$\psi = 30^\circ$
Load data	Prestress	-30 Mpa
	Edge pressure	30 Mpa

Figure 3.12.3
Normalized stress vs. radius obtained using plane strain elements

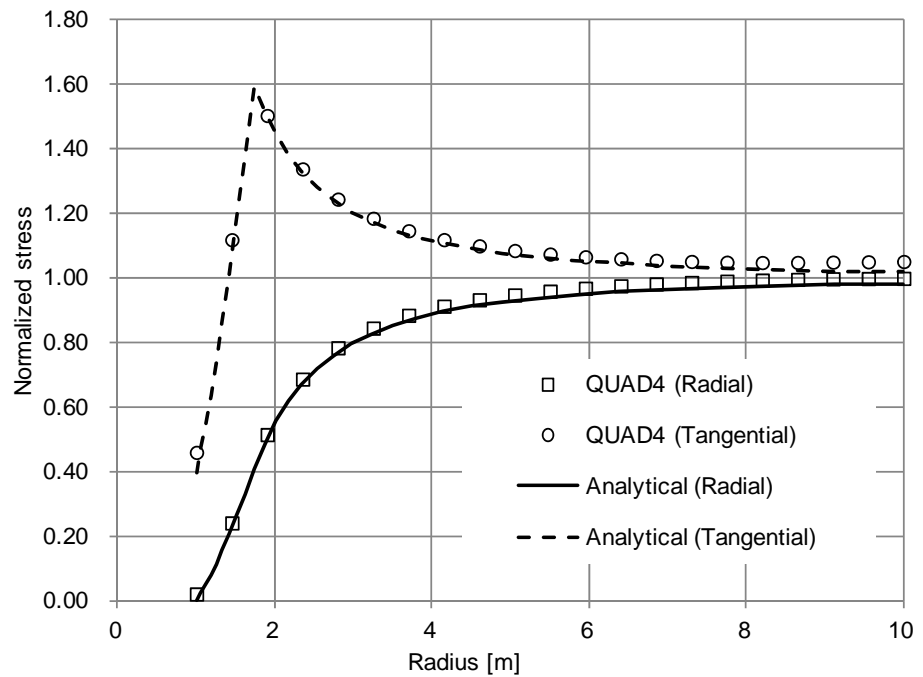




Figure 3.12.4
Normalized displacement vs. radius obtained using plane strain elements

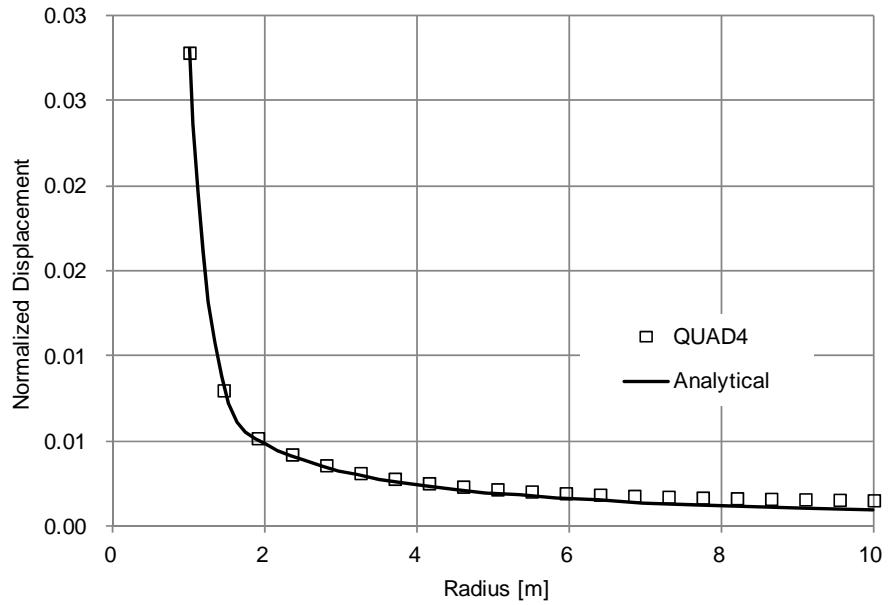


Figure 3.12.5
Normalized stress vs. radius obtained using axisymmetric elements

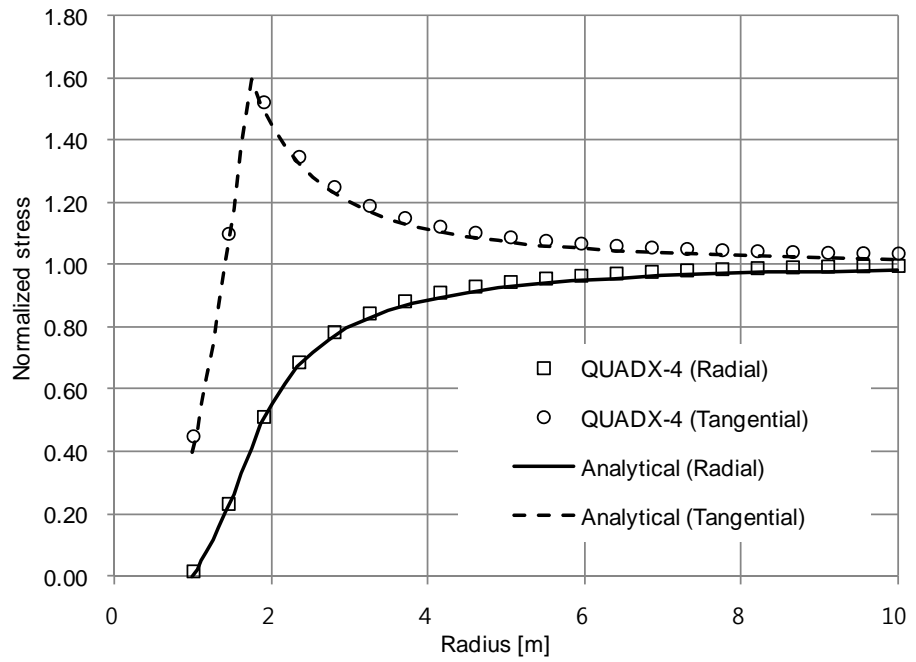




Figure 3.12.6
Normalized displacement vs. radius obtained using axisymmetric elements

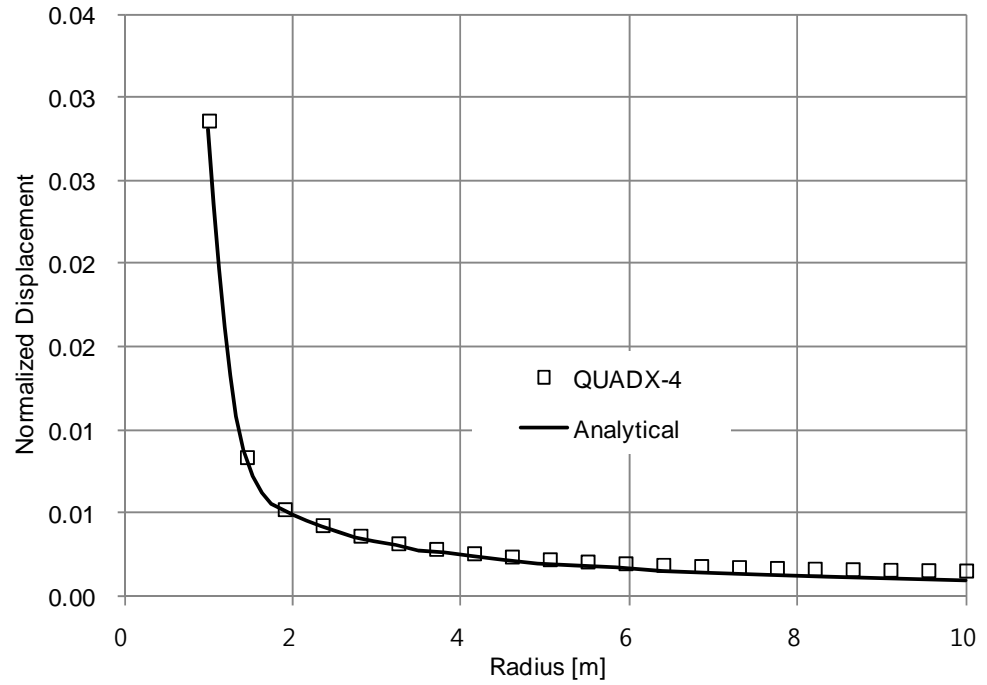


Table 3.12.1 Yield zone radius

	Yield zone radius [m]
Reference	1.731
QUAD-4	1.81
QUADX-4	1.81



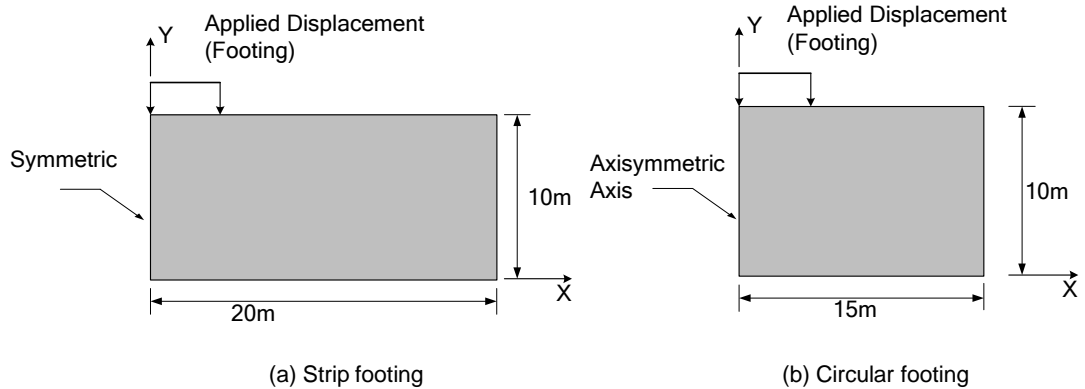
3.13 Strip and Circular Footings on a Mohr-Coulomb Soil

REFERENCE	Terzaghi, K. et al. ¹⁴ , Cox et al. ¹⁵
ELEMENTS	Plane strain elements, solid elements
MODEL FILENAME	Material13_1.gts, Material13_2.gts, Material13_3.gts, Material13_4.gts

Bearing capacity of Mohr-Coulomb soil is evaluated in this problem. Two types of footing conditions are considered: a strip footing and a circular footing. Plane strain and solid elements are utilized to solve the footing problem. Axisymmetric and solid elements are employed for the circular footing problem. Prescribed displacements in the footing area are gradually increased to obtain the limiting footing pressure. Analytic solutions are taken for the standard of comparison.

The bearing pressure for the strip footing problem with friction angle of soil equal to zero can be expressed as $q = (2 + \pi)c$, where c is the cohesion of the material. For the circular footing problem, the semi-analytical solution of the average pressure over the footing at failure for a friction angle of 20° is expressed as $q = 20.1c$.

Figure 3.13.1
Schematic model for strip and circular footing problem



Material data (strip footing)	Young's modulus	$E = 257140 \text{ kPa}$
	Poisson's ratio	$\nu = 0.285714$
	Yield criteria	<i>Mohr-Coulomb</i>
	Cohesion	$c = 100 \text{ kPa}$
	Friction angle	$\phi = 0^\circ$
	Dilatancy angle	$\psi = 0^\circ$



Material data (circular footing)	Young's modulus	$E = 257140 \text{ kPa}$
	Poisson's ratio	$\nu = 0.285714$
	Yield criteria	<i>Mohr-Coulomb</i>
	Cohesion	$c = 100 \text{ kPa}$
	Friction angle	$\phi = 20^\circ$
	Dilatancy angle	$\psi = 20^\circ$

Figure 3.13.2
Pressure vs. vertical displacement response of strip footing problem obtained using plane strain and solid elements

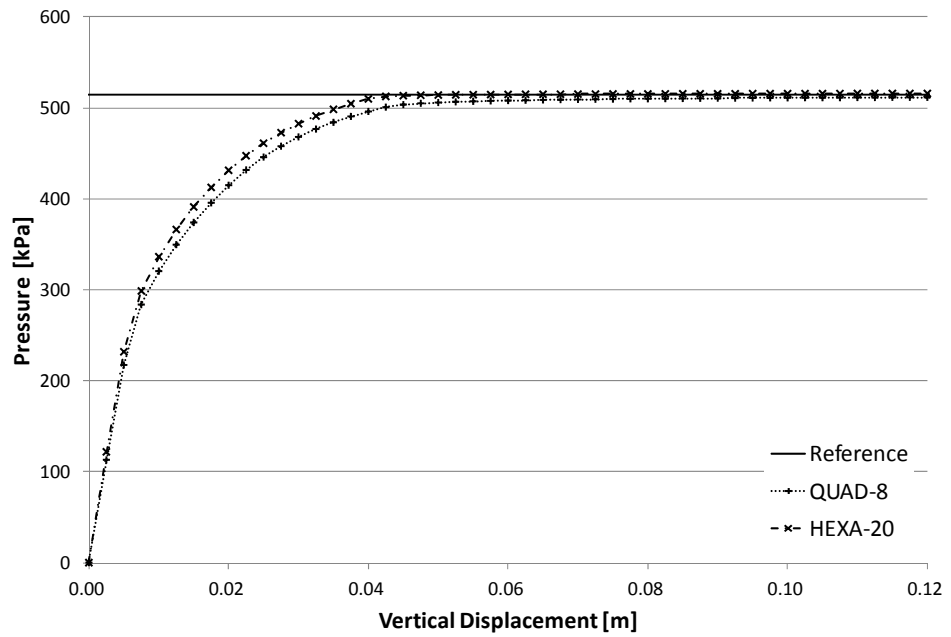
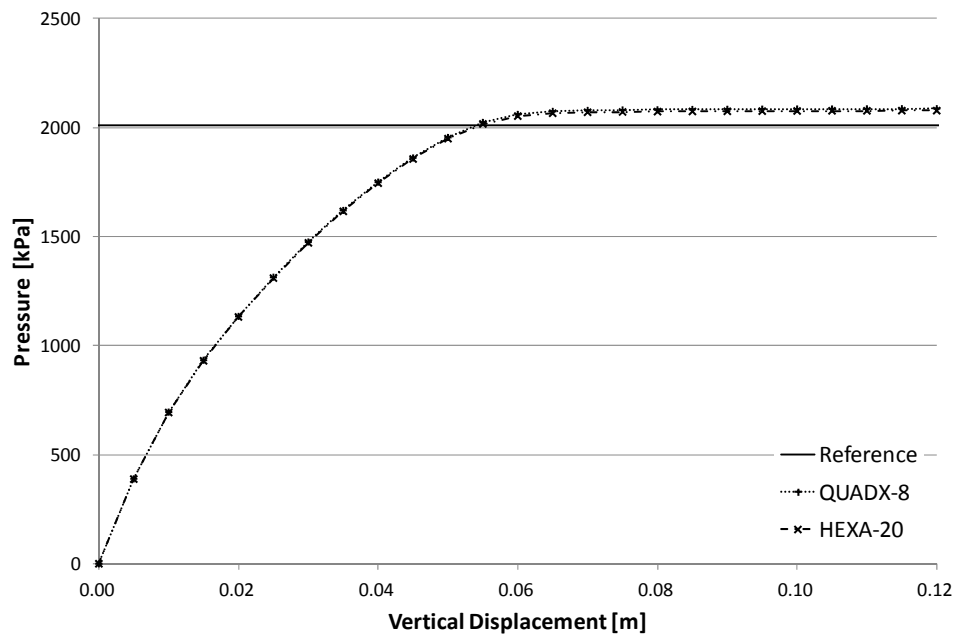


Figure 3.13.3
Pressure vs. vertical displacement response of circular footing problem obtained using axisymmetric and solid elements



*Table 3.13.1 Bearing Capacity of Strip and Circular footings in KPa.*

	Strip Footing	Circular Footing
Reference	514.2	2010.0
QUAD-8	511.62	-
QUADX-8	-	2090.3
HEXA20	515.81	2081.1



3.14 Effect of Strain Rate on Undrained Effective Stress Path and Stress-Strain Response

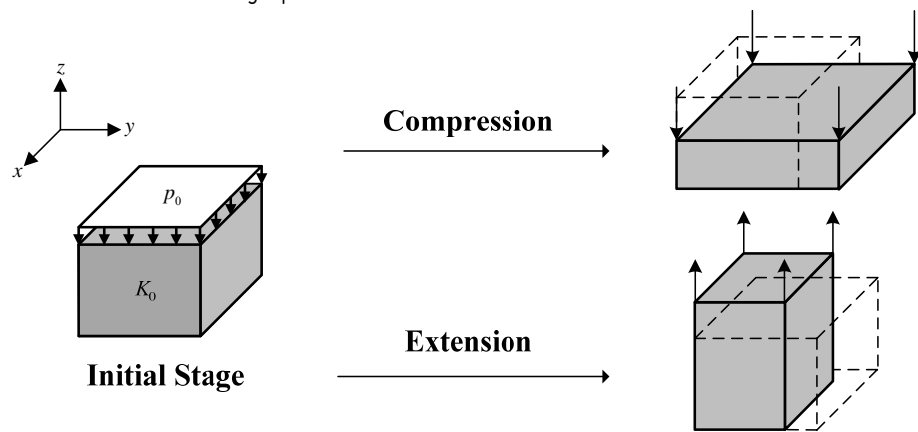
REFERENCE	Sekiguchi, H., et al. ¹⁶
ELEMENTS	Solid elements
MODEL FILENAME	Material14_1.gts, Material14_2.gts

Figure 3.14.1 depicts undrained compression and extension simulations carried out under K_0 consolidated triaxial conditions. Vertical pressure is applied on the upper surface and K_0 condition is applied to reproduce in-situ stresses at initial stage. In the subsequent stage, specified displacement loads are applied in the z-direction with various strain rates to demonstrate the time effects on undrained responses.

Effective stress paths and stress-strain responses are plotted and compared with those from the original Sekiguchi-Ohta model in Figures 3.14.2 and 3.14.3. Dots represent the reference data and the lines are those obtained from the Sekiguchi-Ohta inviscid and viscid models in GTS NX.

Shown in Figure 3.14.2, the undrained strengths, defined as the maximum value of $|\sigma_a - \sigma_r|/2$, are dependent on the strain rates. Also, the paths are asymmetric for compression and extension sides, as are also evident from the reference graphs.

Figure 3.14.1 triaxial compression and extension test configuration



Material data	Poisson ratio	$\nu = 0.3$
	Slope of consolidation line	$\lambda/(1+e_0) = 0.0921$
	Slope of over-consolidation line	$\kappa/(1+e_0) = 0.0199$
	Coefficient of dilatancy	$D = 0.053$
	Secondary compression Coefficient	$\alpha = 0.0029$
	Shear modulus	$G/p_0 = 25$
	Initial volumetric strain ratio	$\dot{v}_0 = 10^{-7}$
	K_0	$K_0 = 0.5$



Figure 3.14.2
Undrained effective stress paths with different strain rates

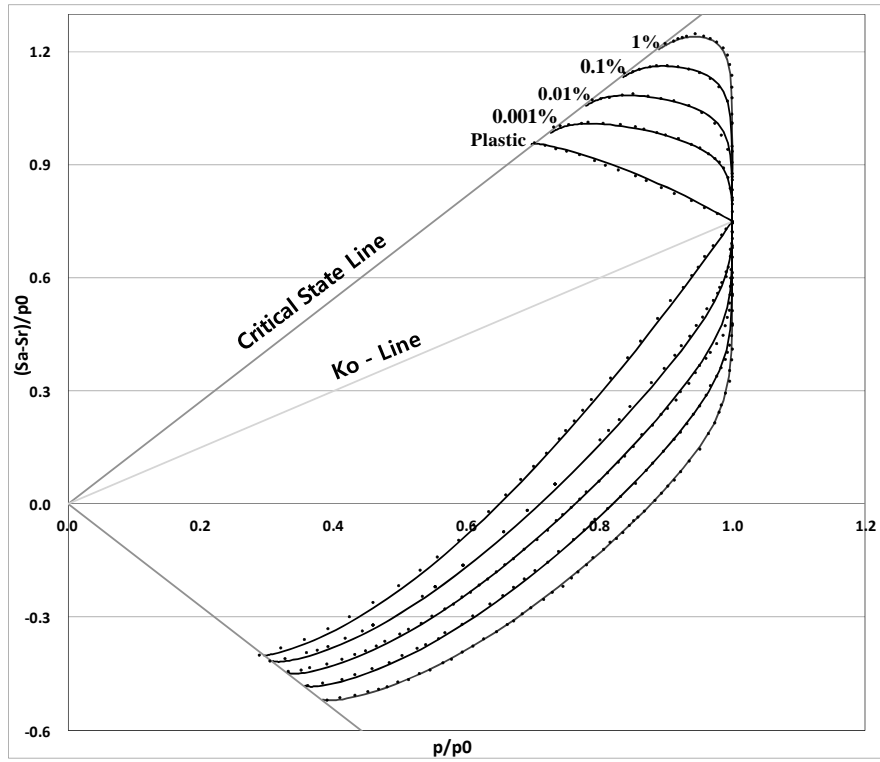
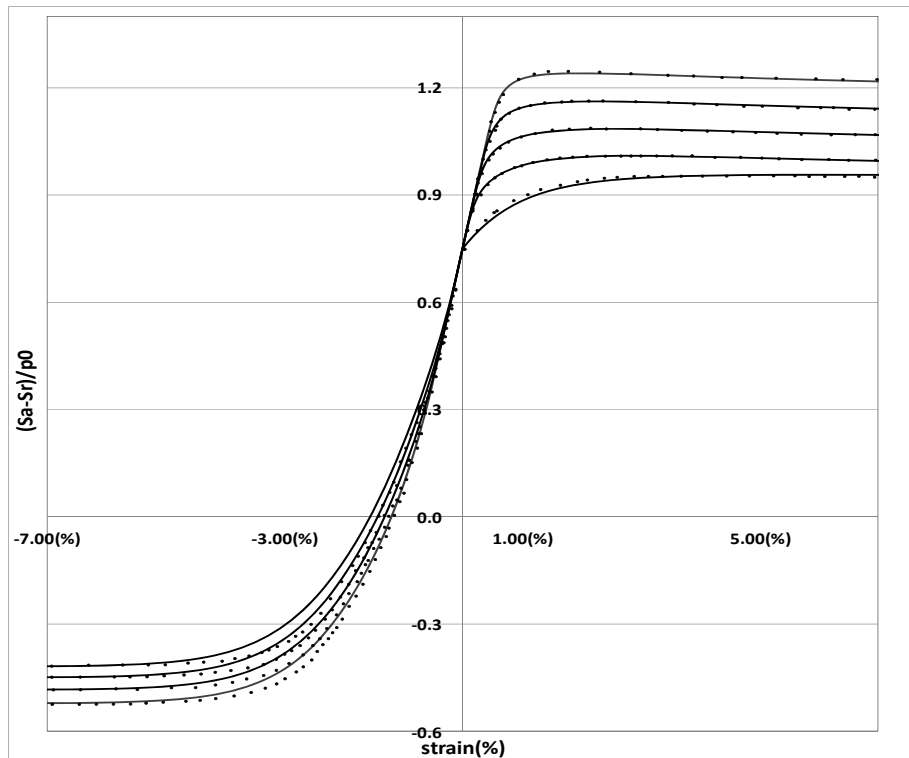


Figure 3.14.3
Undrained stress-strain response with different strain rates





3.15 Oedometer Test for Hardening Soil with Small Strain Stiffness with Drained Condition

REFERENCE	Benz, T. ¹⁷
ELEMENTS	Solid elements
MODEL FILENAME	Material15_1.gts, Material15_2.gts

Oedometer compression tests are carried out using "Hardening soil" material model and "Hardening soil with small strain stiffness" material model with drained condition. Figure 3.15.1 depicts the test configuration and the specimen has unit dimension.

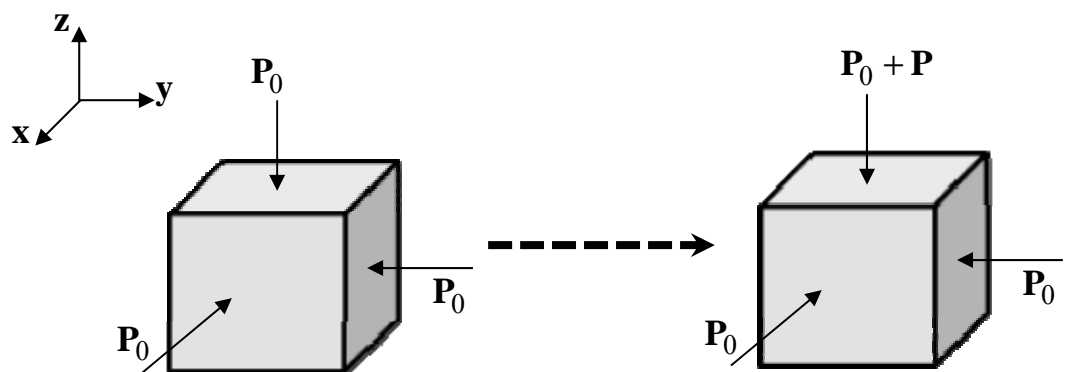
The material table below shows the data of loose and dense "Hostun" sand, used in the simulation. The only differences of "Hardening soil" and "Hardening soil with small strain stiffness" model are "shear modulus at small strain (G0ref)" and "threshold shear strain".

The simulations are carried out with two different material properties. At initial stage, the specimens are loaded with uniform confining pressure 25kPa. In the case of loose "Hostun" sand, the additional pressure along z direction is loaded consecutively to 50kPa, 100kPa, 200kPa with intermediate unloading stages. In the case of dense "Hostun" sand, the additional pressure along z direction is loaded consecutively to 100kPa, 200kPa, 400kPa with intermediate unloading stages.

Figure 3.15.2, 3.15.3 show the results of simulation. The result of the loose "Hostun" sand are shown in the figure 3.16.2 and one of the dense "Hostun" sand are shown in the figure 3.16.2.

The test results show that the "Hardening soil with small strain stiffness" model produce a little stiffer response than "Hardening soil" model. And due to high "threshold shear strain", the difference between models can be seen more clearly in dense sand.

Figure 3.15.1
Oedometer test configuration





Material data	Hostun sand	Loose	Dense
Poisson ratio		0.2	0.2
E50 ref		20000 kPa	40000 kPa
Eoed ref		20000 kPa	40000 kPa
Eur ref		60000 kPa	120000 kPa
Failure ratio		0.9	0.9
Reference pressure		100 kPa	100 kPa
Power of stress level		0.5	0.5
K0nc		0.5	0.36
Friction angle		30. degree	40. degree
Dilatancy angle		0. degree	10. degree
Cohesion		0.	0.
Tensile strength		0. kPa	0. kPa
G0 ref		70000 kPa	122500 kPa
Threshold shear strain		0.0001	0.0002

Figure 3.15.2
Oedometer test on
loose Hostun sand

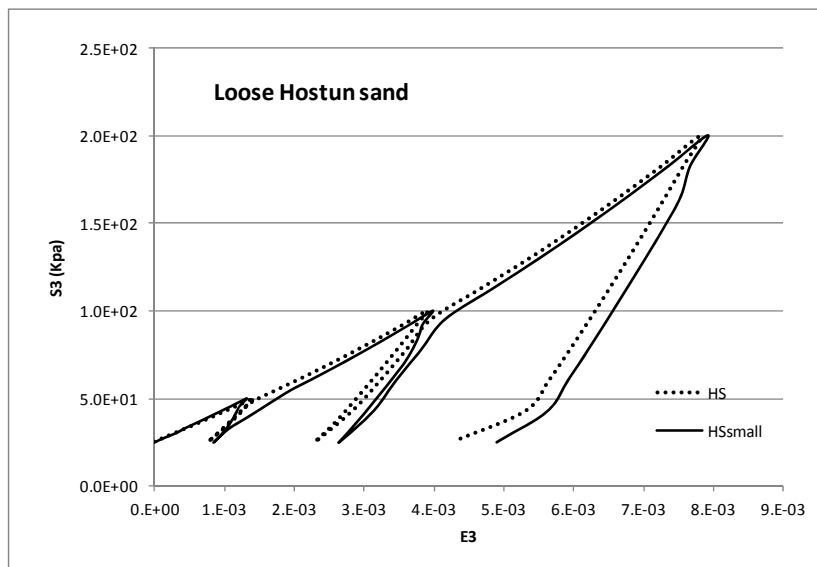
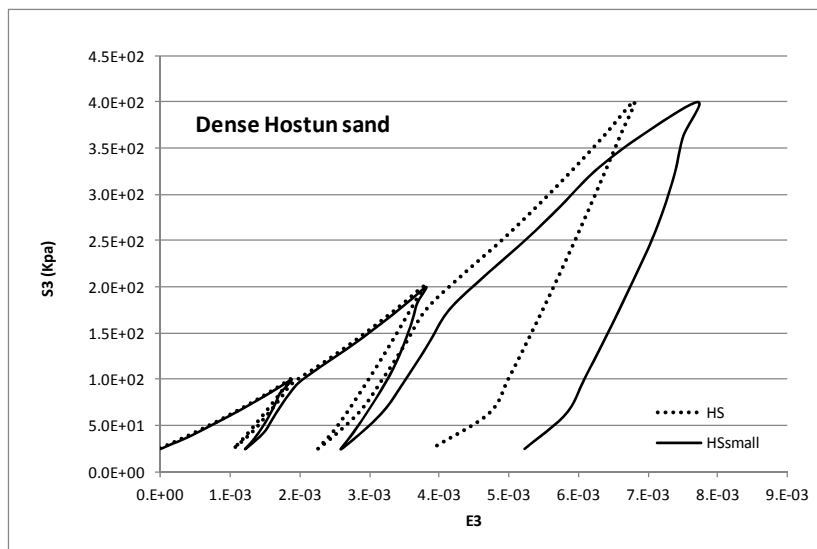


Figure 3.15.3
Oedometer test on
dense Hostun sand





3.16 Triaxial Test for Hardening Soil with Small Strain Stiffness with Drained Condition

REFERENCE	Benz, T. ¹⁷
ELEMENTS	Solid elements
MODEL FILENAME	Material16_1.gts, Material16_2.gts

Triaxial compression tests are carried out using "Hardening soil" material model and "Hardening soil with small strain stiffness" material model with drained condition. Figure 3.16.1 depicts the test configuration and the specimen has unit dimension.

The material table below shows the data of loose and dense "Hostun" sand, used in the simulation. The only differences of "Hardening soil" and "Hardening soil with small strain stiffness" model are "shear modulus at small strain (G0ref)" and "threshold shear strain".

The simulations are carried out with two different material properties and three different initial conditions.. At initial stage, the specimens are loaded with uniform confining pressure 100kPa, 300kPa, 600kPa respectively. And in the subsequent stage, prescribed displacements are loaded along the z-direction.

According to the specification of the material model, the hyperbolic relation between the vertical strain and the deviatoric stress, "q", in triaxial test only works if the "q" is less than the ultimate deviatoric stress, "qf", which comes from the mohr-coulomb model. And if the "q" is more than the "qf", the models works like perfect plastic mohr-columb model.

Figure 3.16.2, 3.16.3, 3.16.4, 3.16.5 show the results of simulation. The results of the loose "Hostun" sand are shown in the figure 3.16.2, 3.16.3, and ones of the dense "Hostun" sand are shown in the figure 3.16.4, 3.16.5.

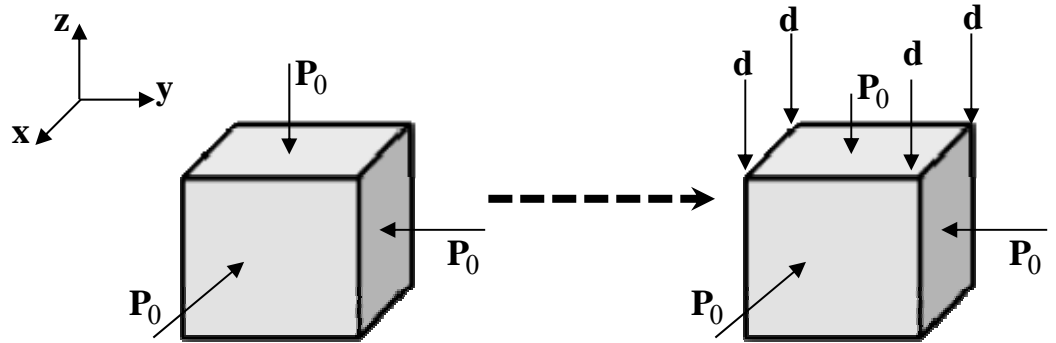
The axial strain vs. stress ratio is compared with the analytical solution of "Hardening soil" model in the figure 3.16.2, 3.16.4. and the analytical solutions are only calculated up to the ultimate deviatoric stress. In the figures, "stress ratio" means the ratio of loading stress along z-direction to confining stress. From the results, it is obvious that perfect yielding occurs above the ultimate deviatoric stress.

The "dense sand" has dilatancy angle and the "loose sand" doesn't. The dilatancy effect can be verified from the results of axial strain vs. volumetric strain shown in the figure 3.16.3, 3.16.5.

All test results show that there are little difference between "Hardening soil" model and "Hardening soil with small strain stiffness" model in triaxial test.



Figure 3.16.1
Triaxial test
configuration



Material data	Hostun sand	Loose	Dense
Poisson ratio		0.2	0.2
E50 ref		20000 kPa	40000 kPa
Eoed ref		20000 kPa	40000 kPa
Eur ref		60000 kPa	120000 kPa
Failure ratio		0.9	0.9
Reference pressure		100 kPa	100 kPa
Power of stress level		0.5	0.5
K0nc		0.5	0.36
Friction angle		30. degree	40. degree
Dilatancy angle		0. degree	10. degree
Cohesion		0.	0.
Tensile strength		0. kPa	0. kPa
G0 ref		70000 kPa	122500 kPa
Threshold shear strain		0.0001	0.0002



Figure 3.16.2.(a)
Axial strain vs. stress ratio of the loose Hostun sand with confining stress 100kPa

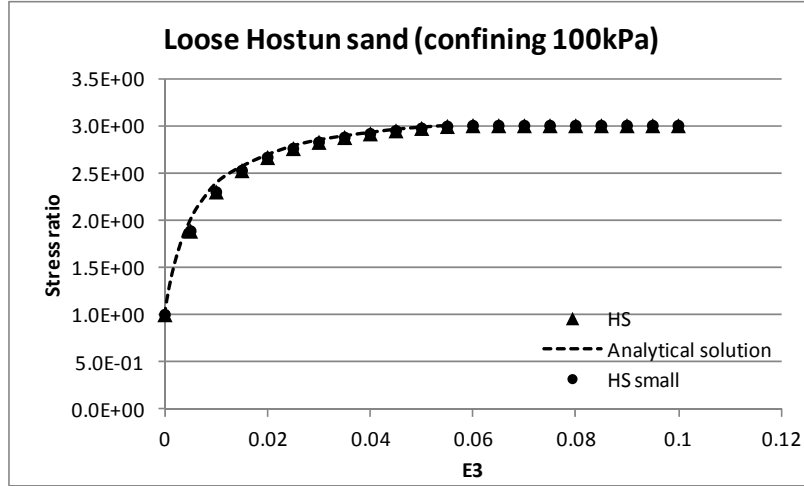


Figure 3.16.2.(b)
Axial strain vs. stress ratio of the loose Hostun sand with confining stress 300kPa

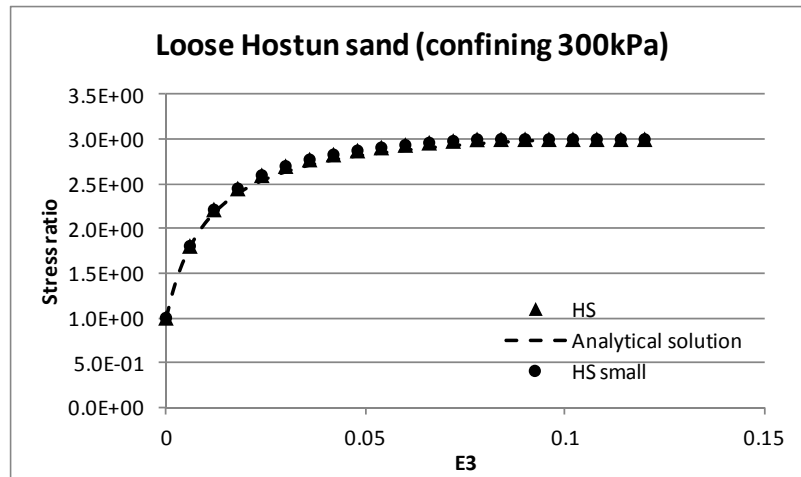


Figure 3.16.2.(c)
Axial strain vs. stress ratio of the loose Hostun sand with confining stress 600kPa

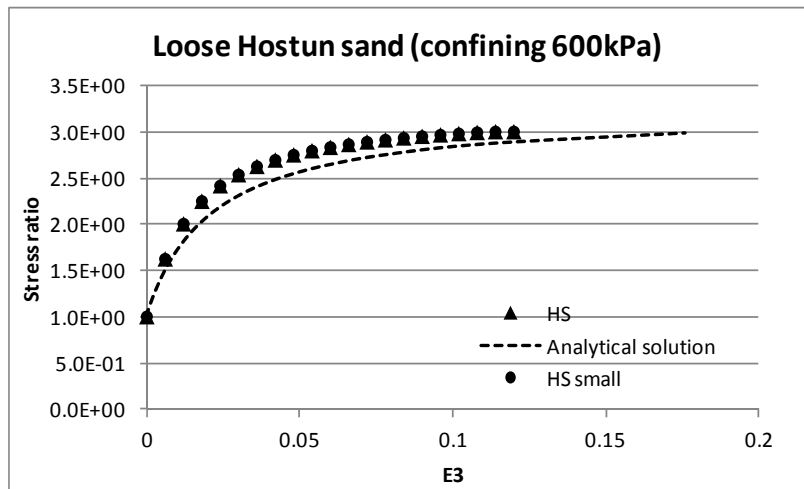




Figure 3.16.3.(a)
Axial strain vs.
volumetric strain of the
loose Hostun sand with
confining stress 100kPa

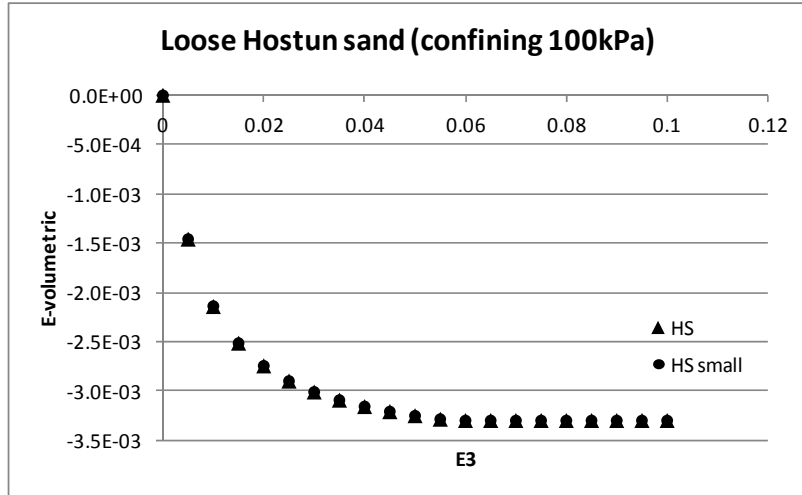


Figure 3.16.3.(b)
Axial strain vs.
volumetric strain of the
loose Hostun sand with
confining stress 300kPa

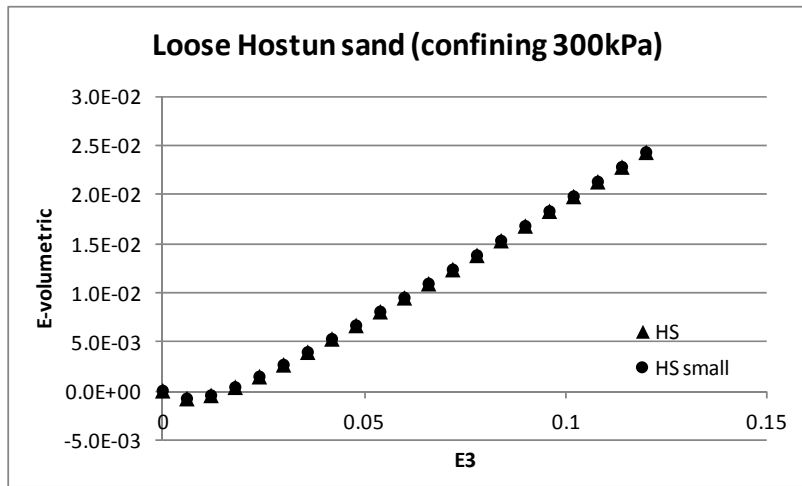


Figure 3.16.3.(c)
Axial strain vs.
volumetric strain of the
loose Hostun sand with
confining stress 600kPa

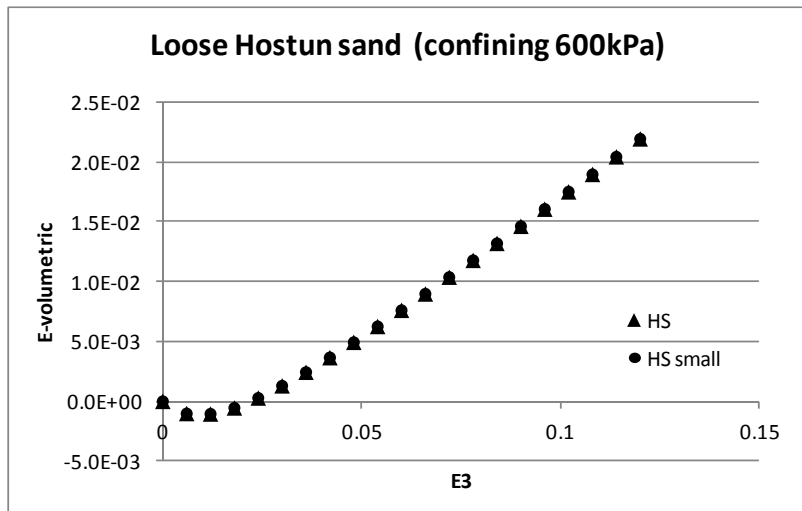




Figure 3.16.4.(a)
Axial strain vs. stress ratio of the dense Hostun sand with confining stress 100kPa

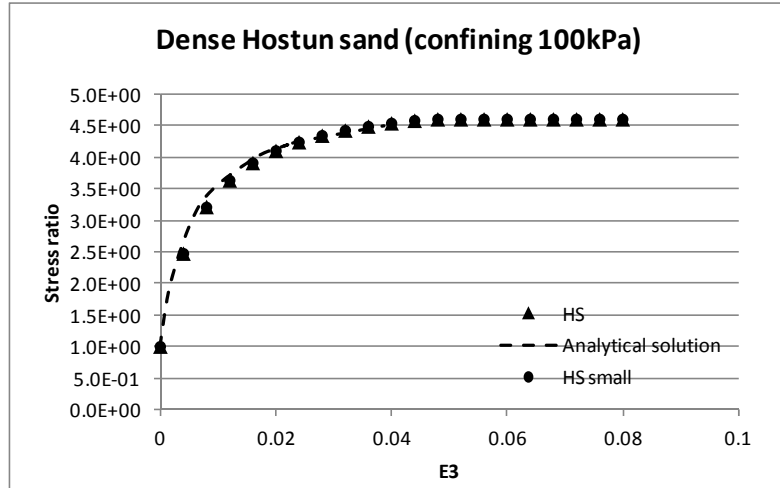


Figure 3.16.4.(b)
Axial strain vs. stress ratio of the dense Hostun sand with confining stress 300kPa

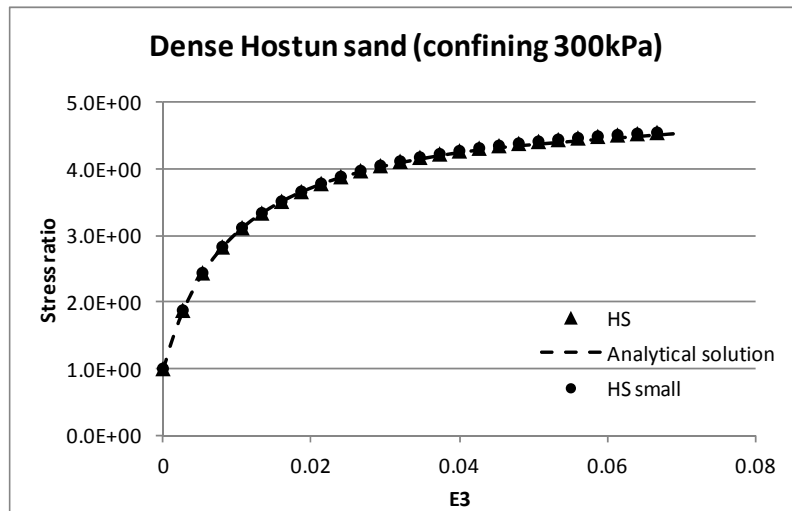


Figure 3.16.4.(c)
Axial strain vs. stress ratio of the dense Hostun sand with confining stress 600kPa

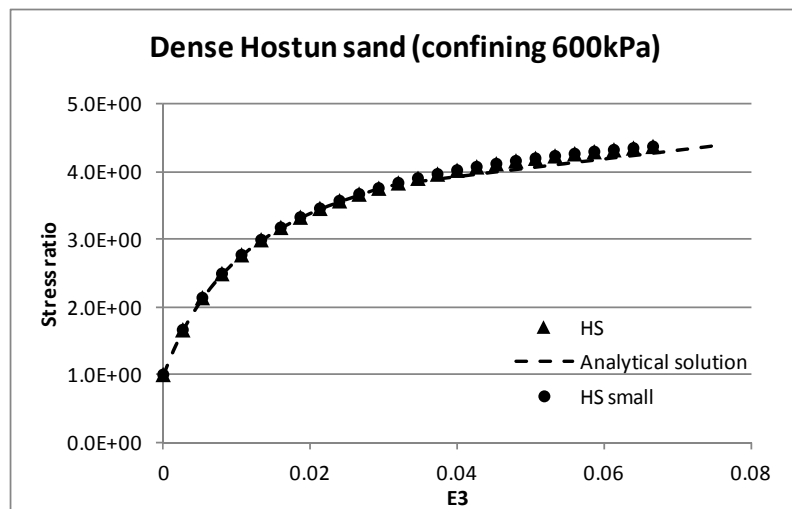




Figure 3.16.5.(a)
Axial strain vs.
volumetric strain of the
dense Hostun sand with
confining stress 100kPa

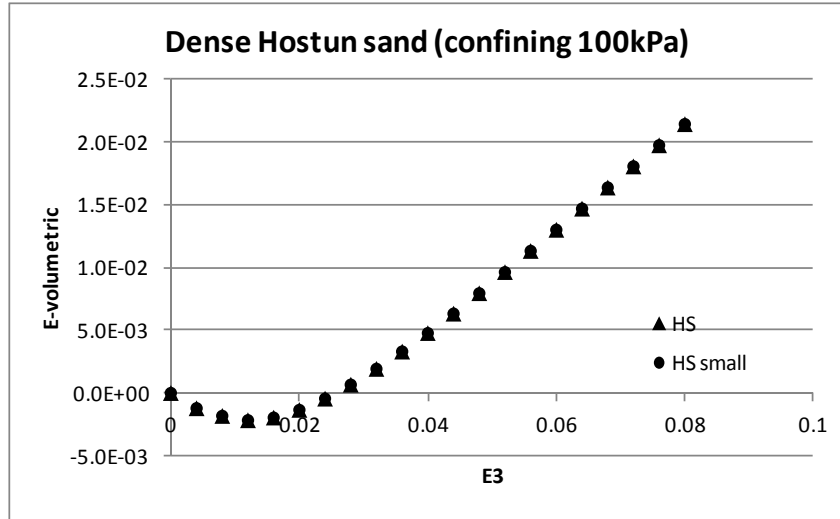


Figure 3.16.5.(b)
Axial strain vs.
volumetric strain of the
dense Hostun sand with
confining stress 300kPa

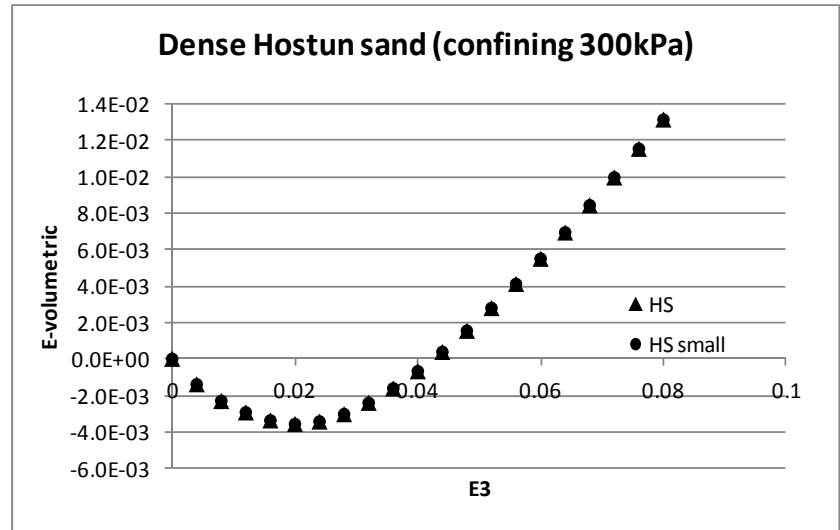
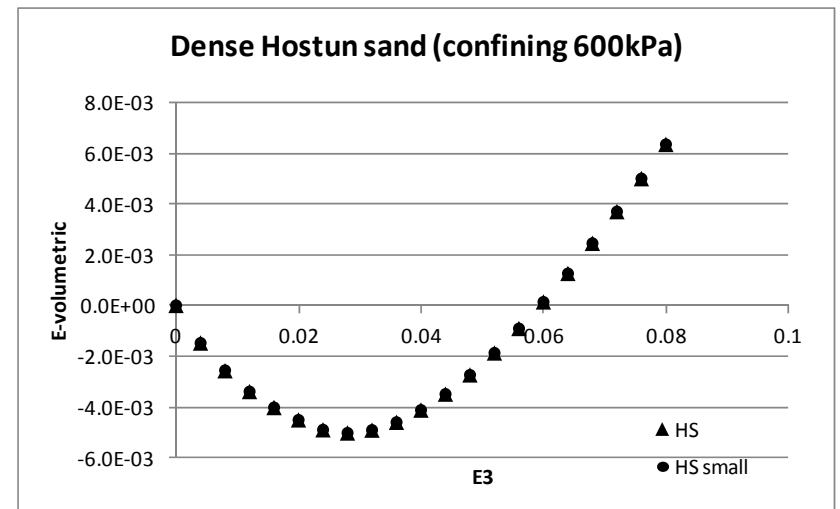


Figure 3.16.3.(c)
Axial strain vs.
volumetric strain of the
dense Hostun sand with
confining stress 600kPa





3.17 Undrained Triaxial Test with SCLAY1 Material Model

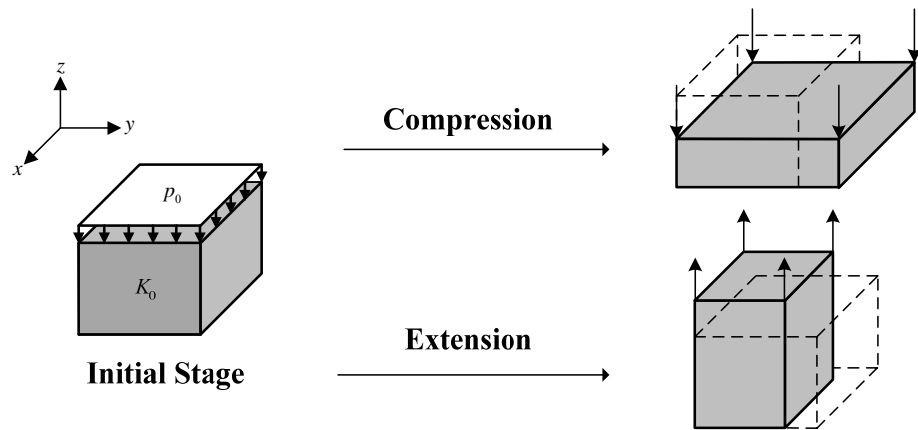
REFERENCE	LEONI, M. ¹⁸
ELEMENTS	Solid element
MODEL FILENAME	Material17_1.gts

SCLAY1 is an elasto-plastic model which accounts for initial stress induced anisotropy and rotational hardening law. Generalized SCLAY1S model available in GTS NX is an advanced version of SCLAY1 model that also accounts for bonding and destructuration law. Generalized SCLAY1S model can be degenerated into SCLAY1 model when parameters related bonding and destructuration law are set to zero.

Undrained triaxial compression and extension simulations are carried out with degenerated Generalized SCLAY1S model to focus on the effect of rotational hardening law. Initially, vertical pressure is applied on the sample and in-situ stresses are generated with K_0 condition. At the subsequent stage, specified displacements in the z-direction are applied to model the compression and extension tests.

Effective stress paths and stress-strain behavior of compression and extension tests are obtained. The results are compared with those from the reference. In Figures 3.17.2 and 3.17.3, the lines represent the data obtained using GTS NX and dots are the reference data. Characteristic responses of the SCLAY1S model are well captured by using GTS NX. Asymmetry of stress paths as depicted in Figure 3.17.2 are mainly attributed to initial stress induced anisotropy. The 'hook' type stress path is usually recognized as a defect of the model in undrained triaxial extension.

Figure 3.17.1. triaxial compression / extension test with K_0 condition



Material data	Poisson ratio	$\nu = 0.255$
	Slope of consolidation line	$\lambda/(1+e_0) = 0.1055$
	Slope of over-consolidation line	$\kappa/(1+e_0) = 0.0161$
	Slope of critical state line	$M = 1.29$
	Degree of anisotropy	$\alpha = 0.493$
	Abs. effectiveness of rotational hardening	$\mu = 28$
	Rel. effectiveness of rotational hardening	$\beta = 0.856$
	K_0	$K_0 = 0.47$



Figure 3.17.2
Undrained effective
stress paths

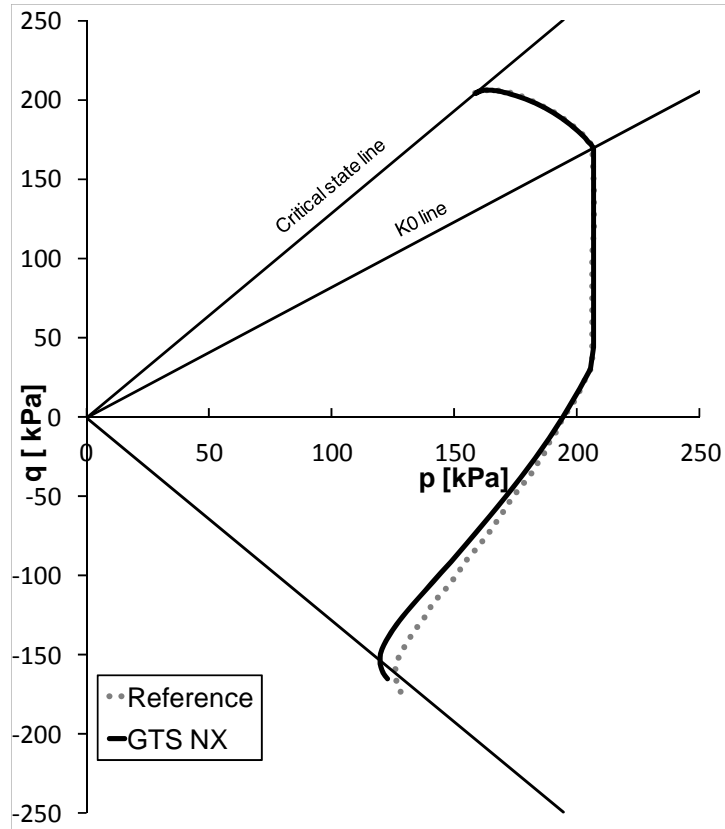
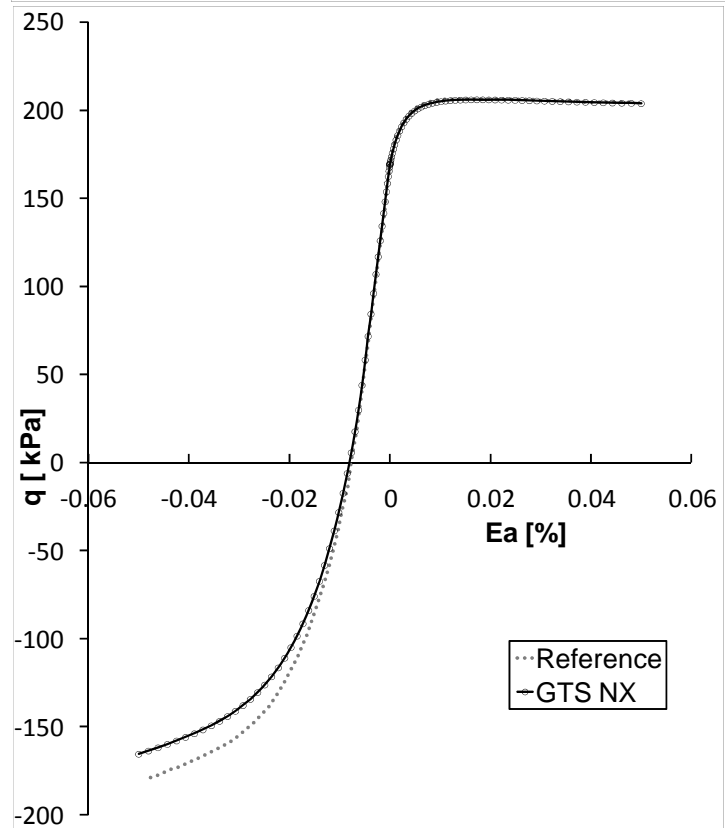


Figure 3.17.3
Undrained stress-
strain responses





3.18 Unit Tests of Coulomb Friction Model for Interface Elements

REFERENCE	Analytical solution
ELEMENTS	Line interface elements, Plane strain elements
MODEL FILENAME	Material18_1.gts, Material18_2.gts

Unit tests are carried out for the coulomb friction model of interface elements.

Figure 3.18.1 depicts the test configuration. In the figure, two quadrilateral blocks mean soil and between them, there are interface elements to correlate. The gap between soil has no physical meaning, but exist for the description of clarity of interface elements.

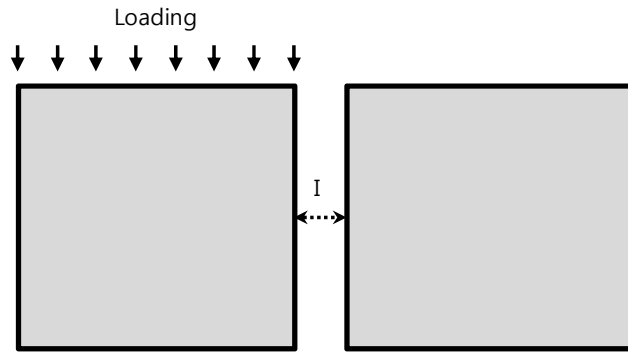


Figure 3.18.1. Unit test configuration

The column friction model is defined as the following formula and for more details, review the reference manual.

$$f = \sqrt{t_r^2} + t_n \tan \phi(\kappa) - c(\kappa) = 0$$

$$g = \sqrt{t_r^2} + t_n \tan \psi$$

The table below show the material data for interface elements.

Material data for pile	Normal stiffness modulus	$K_n = 50.$	kN/m^3
	Shear stiffness modulus	$K_t = 40.$	kN/m^3
	Friction angle	$\phi = 30.$	degree
	Dilatancy angle	$\psi = 0. / 10.$	degree
	Cohesion	$c = 0.04$	kN/m^3
Material data for pile tip	Normal stiffness modulus	$K_n = 50.$	kN/m^3
	Shear stiffness modulus	$K_t = 40.$	kN/m^3
	Friction angle	$\phi = 30.$	degree
	Dilatancy angle	$\psi = 0. / 10.$	degree
	Cohesion		
		Plastic displacement	Cohesion (kN/m^3)
		0.0	0.04
		0.2	1.0



Interface property	Thickness	1.0 m
---------------------------	-----------	-------

The simulations are carried out with respect to the constant cohesion and the plastic dependent cohesion with two dilatancy angles respectively. Soil is loaded using self weight at initial stage and to induce shear stress, the left side soil is loaded with a specified displacement at the subsequent stage.

For the following figure, probing points for interface element results are selected at the 1st node of interface element at the top side soil.

Figure 3.18.2
Unit test for interface elements with constant cohesion

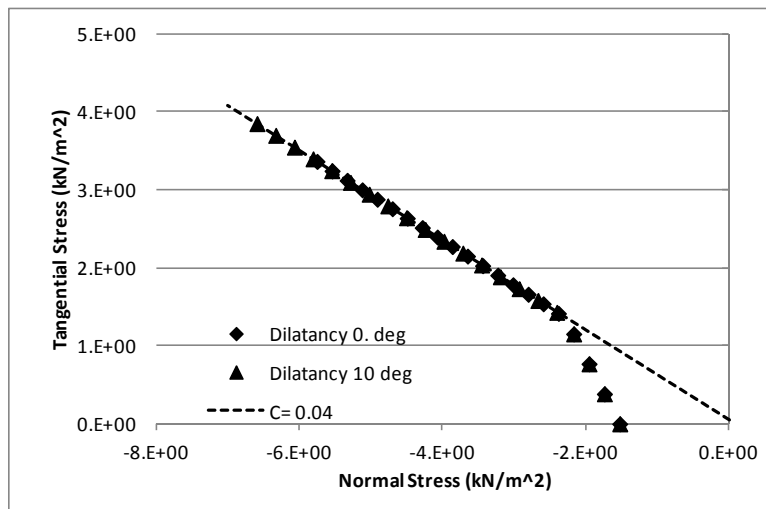
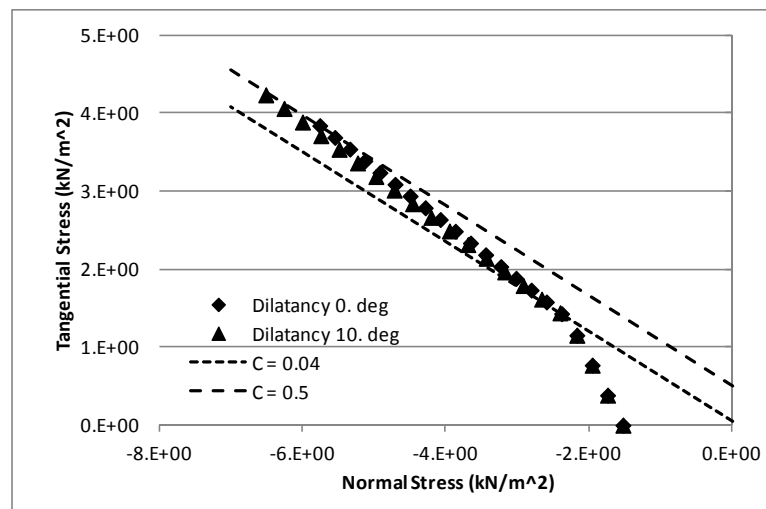


Figure 3.18.3
Unit test for interface elements with plastic dependent cohesion



In the above figure for plastic dependent cohesion, it can be shown that the cohesion grows as plastic relative displacement is increased and the guide line for C=0.5 exist only for the clear explanation purpose.



3.19 Unit Tests for Pile, Pile tip Elements

REFERENCE	Analytical solution
ELEMENTS	Pile , Pile tip elements
MODEL FILENAME	Material19_1.gts, Material19_2.gts

Unit tests are carried out for the nonlinear behavior of pile/pile tip elements.

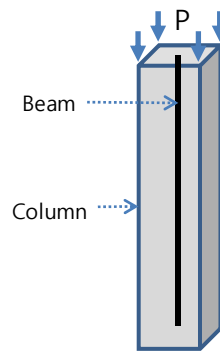
Figure 3.19.1 depicts the test configuration. In the figure, the rectangular column is modeled with solid elements, and the beam inside the rectangular column is modeled with beam elements. Pile elements correlate two element types. Pile tip elements are attached at the end of the pile elements.

The nonlinear behaviors for pile, pile tip elements can be defined as perfect plastically using a ultimate force or to follow multi linear curve using table function. And if a table given, the stiffness for an element is determined according to the slope of the multi linear curve.

The table below show the material data for pile, pile tip elements and the thickness for pile elements.

The simulations are carried out with perfect plastic and a multi linear curve conditions.

Figure 3.19.1.
Unit test configuration



All test results show that pile, pile tip elements exactly follow the given nonlinear behaviors. In the case of perfect plastic for pile elements, analytical solution is 0.15kN/m because of the pile thickness.

Material data for pile	Normal stiffness modulus	$K_n = 80 \text{ kN/m}^3$
	Shear stiffness modulus	$K_t = 100 \text{ kN/m}^3$
	Ultimate shear force	$F_u = 1.5 \text{ kN/m/m}$
	Normal stiffness modulus Table	$K_n = 80 \text{ kN/m}^3$
	Displacement (m)	Force per unit thickness (kN/m/m)
	-0.05	-2.0
	-0.0187	-1.5
	0.0	0.0
	0.0187	1.5
	0.05	2.0



Material data for pile tip	Tip spring stiffness	$K = 100 \text{ kN/m}$	
	Tip bearing capacity	$F_u = 0.4 \text{ kN}$	
	Table	Displacement(m)	Force (kN)
		-0.01	-0.5
		-0.004	0.4
		0.0	0.0
		0.004	0.4
		0.01	0.5
Pile property	thickness	0.1 m	

For the following figure, probing points for pile element results are selected at the 2nd node of pile element at the top.

Figure 3.19.2
Unit test for pile elements

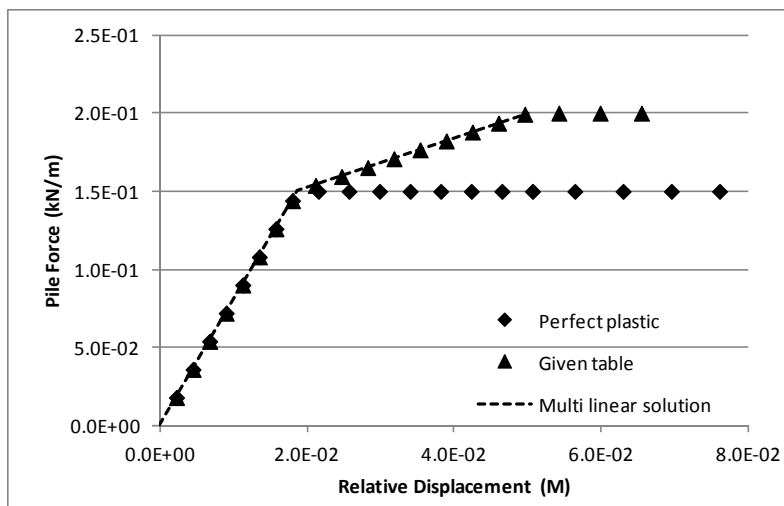
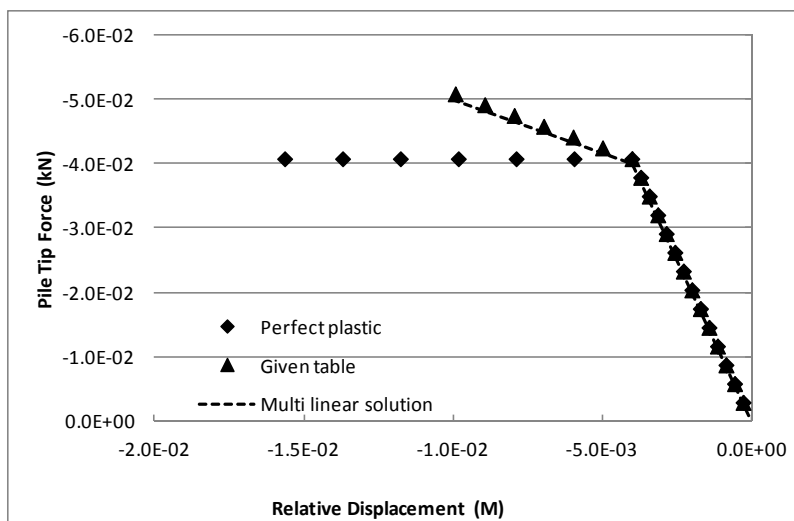


Figure 3.19.3
Unit test for pile tip elements



References

- 1 Sam Helwany, "Applied soil mechanics with ABAQUS applications", John Wiley & Sons, 2007
- 2 Wood, D. M., "Soil Behaviour and Critical State Soil Mechanics.", Cambridge: Cambridge University Press, 1990.
- 3 Hill, R., "The mathematical theory of plasticity", London, Oxford University Press, 1950.
- 4 Green, A. P., "The plastic yielding of notched bars due to bending.", the Quarterly Journal of Mechanics & Applied Mathematics, 6, 223-239, 1953.
- 5 Chakrabarty, J., "Theory of plasticity.", London. McGraw-Hill, 1987.
- 6 Owen, D.R.J. and Hinton, E., "Finite Elements in Plasticity – Theory and Practice", Pineridge Press Limited, Swansea, U.K., 1980.
- 7 Crandall, S. H. and Dahl, N. C., "An Introduction to the Mechanics of Solids", McGraw-Hill Book Co., Inc., New York, NY, 1959
- 8 Green, A. P., "A theory of the plastic yielding due to bending of cantilevers and fixed-ended beams .", Part i. Journal of the Mechanics and Physics of Solid, 3, 1-15, 1954.
- 9 Duncan, J. M. and Chang, C. Y. "Nonlinear Analysis of Stress and Strain in Soils," Journal of the Soil Mechanics and Foundations Division, Vol. 96, No. 5, pp. 1629-1653, 1970.
- 10 Shield, R. T., and Drucker, D. C., "The Application of Limit Analysis to Punch-Indentation Problems." Journal of Applied Mechanics, 20, 453-460, 1953.
- 11 Chen, W. F. "Bearing Capacity of Square, Rectangular and Circular Footings," Limit Analysis and Soil Plasticity, Developments in Geotechnical Engineering 7, Ch. 7, pp. 295-340, New York Elsevier Scientific Publishing Co., 1975.
- 12 Van Langen, H., and Vermeer, P. A., "Interface Elements for Singular Plasticity Points", International Journal for Numerical and Analytical Methods Geomechanics, 15, pp. 301-305, 1991.
- 13 Salencon, J., "Contraction Quasi-Statique D'une Cavite a Symetrie Spherique Ou Cylindrique Dans Un Milieu Elastoplastique," Annales Des Ponts Et Chaussees, No. 4, pp. 231-236, 1969.
- 14 Terzaghi, K., and Peck, R. B., "Soil Mechanics in Engineering Practice", 2nd Edition, John Wiley & Sons, New York, 1967.
- 15 Cox, A. D., Eason, G., and Hopkins, H. G., "Axiially Symmetric Plastic Deformations in Soils", Philosophical Transactions of the Royal Society, S er. A, 254:1, London, 1961.
- 16 Sekiguchi, H., Ohta, H., "Induced anisotropy and time dependency in clays", 9th ICSMFE, Tokyo, Constitutive equations of Soils, 17, 229-238, 1977.
- 17 Benz, T. " Small strain stiffness of soil and its numerical consequences", PhD thesis, University Stuttgart, 2007,
- 18 Leoni, M., KARSTUNEN, M. AND VERMEER, P. A. "anisotropic creep model for creep ", Geotechnique, 58.3, 215-226, 2008